GMTAO

Australian National University

Giant Magellan Telescope Laser Tomography Adaptive Optics Simulation Documentation

Research School of Astronomy and Astrophysics
ANU College of Physical and Mathematical Sciences
The Australian National University

ANU-AO-

Revision History

Version No.	Author & Date	Approval & Date	Description
0.1	P. Piatrou & R. Conan, January 25, 2012		Draft

Contents

List of Tables

List of Figures

1 Modeling of atmospheric turbulence

1.1 Nomenclature

1.2 Atmospheric turbulence statistics for the GMT location

1.3 Random phase screen generation

2 Laser guide star modeling

Laser guide star modeling and propagation to and through telescope is viewed from algorithmic standpoint. The formulas derived herein can be used directly for coding. No approximations are used unless necessary to reduce excessive computational complexity.

The goals of this section are

1. Find wavefront phase map in the telescope entrance pupil given the following set of parameters:
   - laser launch telescope location, pointing and focus position;
   - telescope pointing;
   - position in the telescope entrance pupil.
2. Find spot elongation and orientation in the detector focal plane.
3. Find photon fluxes through the wavefront sensor subapertures.

2.1 Nomenclature

g-system - "global" or "laboratory" coordinate system with respect to which all other coordinates and coordinate systems are defined. Z-axis is along the telescope optical axis at zenith position pointing towards the sky (Fig. 1).

t-system - "telescope" coordinate system such that its z-axis is always along the telescope optical axis for any zenith or azimuth angle.

l-system - "laser launch telescope" coordinate system such that its z-axis is always along the laser launch telescope optical axis.

$(\boldsymbol{o}, \mathcal{R})_b^a$ - the "orientation pair" consisting of the origin coordinate vector $\boldsymbol{o}$ and rotation matrix $\mathcal{R}$ to specify coordinate transformation from coordinate system a to coordinate system b or, in other words, origin and ort coordinates of b-system written in a-system.

h_0, h_+, h_- - median, upper and lower altitudes of the `Na` layer, [m].

$\texttt{Eu}(\alpha, \beta, \gamma)$ - coordinate rotation by Euler angles α, β, γ, [rad].

β_t^g - zenith angle of telescope with respect to g-system, [rad].

β_l^t - zenith angle of the l^{th} LGS with respect to t-system, [rad].

$\boldsymbol{r}_l^t$ - coordinates of l^{th} Laser Launch Telescope (LLT) projected to the telescope Entrance Pupil (EnP), [m].

$\boldsymbol{r}_p^t$ - coordinates of p^{th} point in the EnP grid, [m].

$\boldsymbol{r}_{li}^l$ - coordinates of i^{th} point source in the l^{th} Laser Guide Star (LGS), in l-system, [m].

r_{lip} - distance from i^{th} point source in the l^{th} LGS to p^{th} point in EnP, [m].

Φ_{li} - photon flux from i^{th} point source belonging to l^{th} LGS, [photons].

s^{Na} - sodium coupling efficiency, [(photons m^2)/(s W atom)].

C^{Na} - sodium abundance, [atoms/m^2].

λ - wavelength, [m].

$k = \frac{2\pi}{\lambda}$ - wave number, [rad/m].

2.2 LGS propagation geometry

Geometry of the LGS propagation problem is presented on Fig. 1. The parameters describing the problem are chosen to 1) be close to the ones directly measurable on real telescope, 2) be able to describe quite general situation.

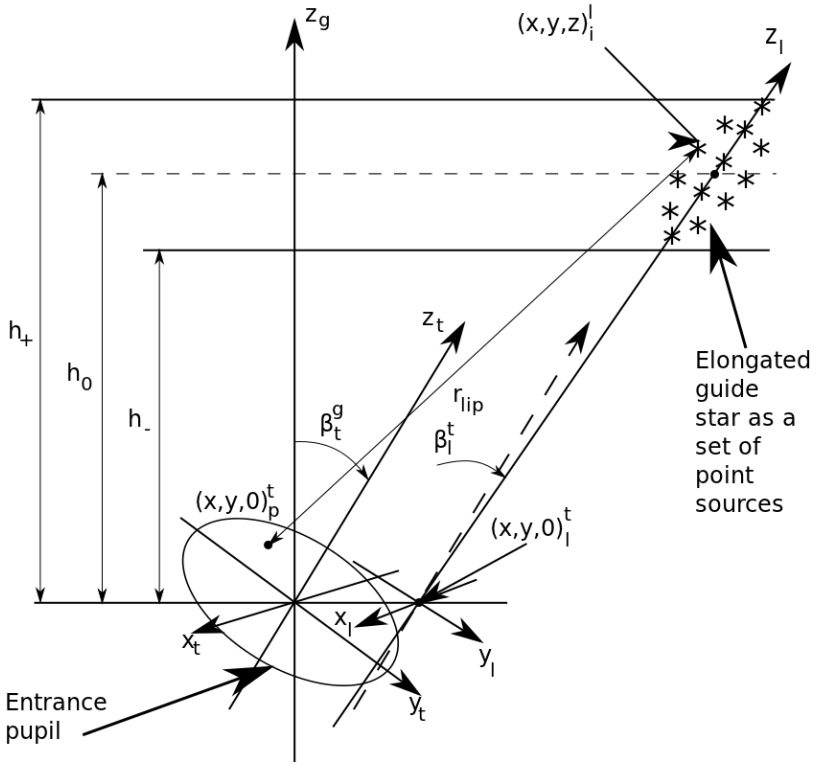

Figure 1: Geometry of laser guide star propagation to the telescope entrance pupil.

Three coordinate systems are involved:

1. Global or g-system is the Cartesian coordinate system with respect to which all other coordinate systems are defined. The orientation pair $(\boldsymbol{o}, \mathcal{R})^0_g$ for this system is just $(\mathbf{0}, \mathcal{I})$.

2. Telescope or t-system is the local Cartesian coordinate system rotating with respect to the g-system such that the t-system z-axis is always along the telescope optical axis. The orientation pair $(\boldsymbol{o}, \mathcal{R})^g_t$ for this system describes the telescope pointing. If we assume that at zenith pointing the t-system coincides with the g-system, then

$$\boldsymbol{o}^g_t = \boldsymbol{o}^0_g = \mathbf{0}, \tag{2.2.1}$$

$$\mathcal{R}^g_t = \mathtt{Eu}(\alpha^g_t, \beta^g_t, 0), \tag{2.2.2}$$

where Euler angles α_t^g, β_t^g have meaning of the telescope azimuth and zenith angles measured with respect to the g-system (note the g superscript). The standard Euler rotation is

$$\mathtt{Eu}(\alpha,\beta,\gamma) = \mathcal{A}_z(\alpha)\mathcal{A}_y(\beta)\mathcal{A}_z(\gamma), \tag{2.2.3}$$

$$\mathcal{A}_z(\alpha) = \begin{bmatrix} \cos\alpha & -\sin\alpha & 0 \\ \sin\alpha & \cos\alpha & 0 \\ 0 & 0 & 1 \end{bmatrix},$$

$$\mathcal{A}_y(\beta) = \begin{bmatrix} \cos\beta & 0 & \sin\beta \\ 0 & 1 & 0 \\ -\sin\beta & 0 & \cos\beta \end{bmatrix}.$$

Coordinates of point p in the entrance pupil given in t-system are $[x,y,0]_p^t = \boldsymbol{r}_p^t$.

3. Laser launch telescope or l-system is a local Cartesian coordinate system chosen such that its z-axis is always along the optical axis of the LLT. This system is naturally defined with respect to the t-system because the LLT is mounted on the moving main telescope mount:

$$(\boldsymbol{o},\mathcal{R})_l^t = ([x,y,0]_l^t, \mathtt{Eu}(\alpha_l^t,\beta_l^t,0), \tag{2.2.4}$$

where $[x,y,0]_l^t = \boldsymbol{r}_l^t$ are the l^{th} LLT location in t-system (pupil coordinates), α_l^t, β_l^t are the azimuth and zenith angles of the LLT orientation with respect to the main telescope optical axis. Note that, for simplicity, we count one LGS per one LLT. In reality one LLT of GMT will generate a pair of LGSs. To account for this we simply assume that there are two differently oriented virtual LLTs at the location of one real LLT.

The LGS is modeled as a combination of the point sources (PSR) distributed within the `Na` layer. Coordinates $\boldsymbol{r}_{li}^l$, $l = 1,...,\#LLT$, $i = 1,...,\#PSR$ of the sources are given in the l-system.

Given orientation pair $(\boldsymbol{o},\mathcal{R})_b^a$ defining b-system coordinates with respect to a-system coordinates, the transformation of coordinates written in b-system into the same coordinates written in a-system is the *direct affine transform*:

$$\boldsymbol{r}^a = \mathcal{R}_b^a \boldsymbol{r}^b + \boldsymbol{o}_b^a. \tag{2.2.5}$$

Correspondingly, the *inverse affine transform* gives the coordinates written in b-system from the ones written in a-system:

$$\boldsymbol{r}^b = (\mathcal{R}_b^a)^T(\boldsymbol{r}^a - \boldsymbol{o}_b^a). \tag{2.2.6}$$

2.3 Finding LGS spot elongation and orientation on the detector

An important geometrical calculation needed for the theoretical evaluation of the detector noise covariance matrix is to find the parameters of the elongated LGS image in the detector focal plane.

Let a LGS is produced as a light-emitting column of length L inside the `Na` layer. We need to find the length of its image in the Shack-Hartmann WFS focal plane behind a lenslet with location $\boldsymbol{r}_l^t$ (in the t-system) projected on the telescope entrance pupil and the image orientation with respect to the detector pixel grid. Let the beginning and end of the LGS light column have t-system coordinates $\boldsymbol{r}_1^t$ and $\boldsymbol{r}_2^T$, respectively. Consider vectors $\boldsymbol{r}_{1t}^t = \boldsymbol{r}_1^t - \boldsymbol{r}_l^t$ and $\boldsymbol{r}_{2t}^t = \boldsymbol{r}_2^t - \boldsymbol{r}_l^t$. Then, up to a scaling factor and a possible mirror flip, the LGS image on the detector is determined by a (ε,θ)-pair, where ε is the angular size of the LGS column as seen from the lenslet center $\boldsymbol{r}_l^t$, that is, the angle between vectors $\boldsymbol{r}_{1l}^t$ and $\boldsymbol{r}_{2l}^t$, and θ is the angle between the t-system x-axis and the line of intersection of the t-system xy-plane and the plane made by vectors $\boldsymbol{r}_{1l}^t$ and $\boldsymbol{r}_{2l}^t$. Vectors $\boldsymbol{r}_{1,2}$ are most conveniently definable in the l-system, where

$$\boldsymbol{r}_{1,2}^l = [0\,0\,z_{1,2}^l]^T. \tag{2.3.1}$$

The transformation to t-system is

$$\boldsymbol{r}_{1,2}^t = \mathcal{R}_l^t \boldsymbol{r}_{1,2}^l + \boldsymbol{o}_l^t. \tag{2.3.2}$$

Using scalar and vector products we get

$$\hat{\boldsymbol{r}}^t_{1,2} = \frac{\boldsymbol{r}^t_{1,2}}{|\boldsymbol{r}^t_{1,2}|}, \tag{2.3.3}$$

$$\cos\varepsilon = \hat{\boldsymbol{r}}^t_1 \cdot \hat{\boldsymbol{r}}^t_2, \tag{2.3.4}$$

$$\boldsymbol{p}^t_{12} = \hat{\boldsymbol{r}}^t_1 \times \hat{\boldsymbol{r}}^t_2, \tag{2.3.5}$$

$$\sin\varepsilon = |\boldsymbol{p}^t_{12}|, \tag{2.3.6}$$

$$\hat{\boldsymbol{p}}^t_{12} = \frac{\boldsymbol{p}^t_{12}}{\sin\varepsilon}, \tag{2.3.7}$$

$$\hat{\boldsymbol{x}}^t = [1\,0\,0]^T, \tag{2.3.8}$$

$$\cos\theta = \hat{\boldsymbol{x}}^t \cdot \hat{\boldsymbol{p}}^t_{12}, \tag{2.3.9}$$

$$\sin\theta = |\hat{\boldsymbol{x}}^t \times \hat{\boldsymbol{p}}^t_{12}|. \tag{2.3.10}$$

Note that, since ε is very small, in order to preserve accuracy, all calculations need to be done in double precision.

2.4 Free-space propagation from LGS to telescope entrance pupil

The electric field E from the LGS on the telescope entrance pupil is the superposition of spherical waves emitted from each point source (PS) that makes the elongated laser guide star spot in the `Na` layer:

$$E_{lp} = \sum_{i=1}^{\#PSR} w_{li} \frac{\exp(ikr_{lip})}{r_{lip}}, \tag{2.4.1}$$

where w_{li} is the weight describing relative intensity of the i^{th} PS of the l^{th} LGS, r_{lip} is the distance from the i^{th} PS of the l^{th} LGS to p^{th} point in the telescope entrance pupil. This distance is easily found through the affine transform:

$$\begin{aligned} \boldsymbol{r}^t_{li} &= \mathcal{R}^t_l \boldsymbol{r}^l_{li} + \boldsymbol{o}^t_l, \\ r_{lip} &= |\boldsymbol{r}^t_{li} - \boldsymbol{r}^t_p|. \end{aligned} \tag{2.4.2}$$

2.5 Geometrical optics propagation through atmosphere

The turbulent atmosphere on the way between an LGS and a telescope is modeled as a set of infinitely thin random *phase screens* (PS) . Because of small phase perturbations caused by each layer and because the typical scale of turbulence is much larger than a wavelength the geometrical optics model for propagation through the layers is assumed. The model is based on the following postulates:

- The propagation of the electromagnetic waves is treated as propagation of *rays* that are normals to the constant phase surfaces of the waves, the *wavefronts*.
- Rays are always straight: the phase screens are weak enough for not to change direction of rays, they only add a path difference $\delta r_{lip,j}$:

$$\begin{aligned} \delta r_{lip,j} &= \phi_{lip,j}/k,\ j = 1, ..., \#PS, \\ r^{turb}_{lip} &= r^{free}_{lip} + \sum_{j=1}^{\#PS} \delta r_{lip,j}. \end{aligned} \tag{2.5.1}$$

  where $\phi_{lip,j}$ is the phase on the j^{th} turbulent layer intersected by a ray emitting from i^{th} point source of l^{th} LGS towards p^{th} point in the entrance pupil. So, the electric field on the entrance pupil will be

$$E^{turb}_{lp} = \sum_{i=1}^{\#PSR} w_{li} \frac{\exp(ikr^{turb}_{lip})}{r^{free}_{lip}}. \tag{2.5.2}$$

Thus, it is necessary to find the intersection of a ray with a turbulent layer.

2.5.1 Turbulence layers are perpendicular to the telescope optical axis.

Assume that the turbulence layers are chosen such that they are perpendicular to the telescope optical axis regardless of the pointing. In this case the turbulence strength depends on the azimuth angle β_t^g, namely,

$$C_n^2(\beta_t^g) = \frac{C_n^2(0)}{\cos\beta_t^g}. \tag{2.5.3}$$

Simple geometrical analysis gives for the relationship between the pupil and turbulence layer coordinates:

$$\boldsymbol{r}_{lip,j}^t = \frac{h_j}{z_{li}^t}\boldsymbol{r}_p^t + (1-\frac{h_j}{z_{li}^t})\begin{bmatrix} x_{li}^t \\ y_{li}^t \\ 0 \end{bmatrix},\ \boldsymbol{r}_{li}^t = \begin{bmatrix} x_{li}^t \\ y_{li}^t \\ z_{li}^t \end{bmatrix}, \tag{2.5.4}$$

where h_j is distance between the telescope and j^{th} phase screen along the telescope optical axis, $\boldsymbol{r}_{lip,j}^t$ are xyz-coordinates in t-system of an intersection point on phase screen j for a ray emitting from i^{th} point source of l^{th} LGS with t-coordinates $\boldsymbol{r}_{li}^t$ and passing through p^{th} point in telescope entrance pupil with t-coordinates $\boldsymbol{r}_p^t$. For the source at infinity (a natural guide star or a scientific target) Eq. (2.5.4) simplifies to

$$\boldsymbol{r}_{lip,j}^t = \begin{bmatrix} \cos\alpha_{li}^t \\ \sin\alpha_{li}^t \\ 0 \end{bmatrix} h_j \tan\beta_{li}^t + \boldsymbol{r}_p^t, \tag{2.5.5}$$

where $(\alpha,\beta)_{li}^t$ are the angular coordinates (first and second Euler angles) of the light source. Note that in both cases the position of the ray intersection with a layer can be written as $(a\boldsymbol{r}_p^t + \boldsymbol{b}_{li}^t)$.

2.5.2 Turbulence layers are parallel to the ground.

Assume that the layers are parallel to the ground, i.e. perpendicular to the g-system's z-axis, and have altitudes $h_j,\ j = 1,...,\#PS$. In this case the turbulence C_n^2 profile is not altered with the zenith angle. Direct ray tracing technique is used to find intersection with a turbulence layer.

Coordinates of a ray can be described through the parametric equation:

$$\boldsymbol{r}(t) = \boldsymbol{i}t + \boldsymbol{r}_0, \tag{2.5.6}$$

where $\boldsymbol{r}_0$ is the ray origin (position of the light-emitting source), $\boldsymbol{i}$, $|\boldsymbol{i}| = 1$ is the ray direction vector, t is the ray path length. In the case of propagation path shown of Fig. 1

$$\boldsymbol{r}_0^l = \boldsymbol{r}_{li}^l,$$

where $\boldsymbol{r}_0$ is given in l-system,

$$\boldsymbol{i}^t = \frac{\boldsymbol{r}_p^t - \boldsymbol{r}_{li}^t}{|\boldsymbol{r}_p^t - \boldsymbol{r}_{li}^t|},$$

where $\boldsymbol{i}$ is given in t-system. Since the turbulent layers are most conveniently defined in the g-system, the ray coordinates need to be transformed into g-system:

$$\begin{aligned} \boldsymbol{r}_0^t &= \mathcal{R}_l^t\boldsymbol{r}_0^l + \boldsymbol{o}_l^t, \\ \boldsymbol{i}^t &= \frac{\boldsymbol{r}_p^t - \boldsymbol{r}_0^t}{|\boldsymbol{r}_p^t - \boldsymbol{r}_0^t|}, \\ \boldsymbol{r}_0^g &= \mathcal{R}_t^g\boldsymbol{r}_0^t + \boldsymbol{o}_t^g, \\ \boldsymbol{i}^g &= \mathcal{R}_t^g\boldsymbol{i}^t. \end{aligned} \tag{2.5.7}$$

The coordinates of ray intersection with turbulent layer are found by equating z-coordinate of a ray to the layer altitude:

$$t = \frac{h_j - r_{0z}^g}{i_z^g}, \tag{2.5.8}$$

$$\boldsymbol{r}^g_{lip,j} = \boldsymbol{i}^g t + \boldsymbol{r}^g_0,$$

where x- and y-coordinates of the $\boldsymbol{r}^g_{lip,j}$-vector are used to find the phase $\phi^{turb}(\boldsymbol{r}^g_{lip,j}) = k\delta r^{turb}_{lip,j}(\boldsymbol{r}^g_{lip,j})$ on the phase screen corresponding to the ray intersection and substitute it to Eq. (2.5.2).

2.6 Point source distribution in the LGS

TBC

The positions $\boldsymbol{r}^l_{li}$ and weights w_{li} of point sources making each LGS are found from superposition of the intensity distribution of the laser radiation forward-propagated through atmosphere to the `Na` layer and the vertical distribution of the `Na` density. A possible operation flow for defining the LGS distribution is the following:

1. Define a 3D mesh covering a part of the `Na` layer penetrated by the laser radiation. Each cell of this mesh is an elementary volume for which amount of laser flux is assigned.

2. Center of each 3D mesh cell is the candidate location of the LGS point source. If flux through the cell exceeds a threshold, a point source is assigned for this cell.

3. For each mesh cell for which a point source is assigned multiply the cell flux by `Na` density at the cell center taken from the `Na` vertical profile. Find relative distribution of the return flux, which is the source weights $\{w_{li}\}_{i=1}^{\#PSR}$:

$$w_{li} = \frac{\Phi_{li} C^{\mathtt{Na}}_{li}}{\sum_{i=1}^{\#PSR} \Phi_{li} C^{\mathtt{Na}}_{li}},\ i = 1, ..., \#PSR \tag{2.6.1}$$

   where $\{\Phi_{li}\}_{i=1}^{\#PSR}$ are the cell fluxes, $\{C^{\mathtt{Na}}_{li}\}_{i=1}^{\#PSR}$ are the `Na` abundances at the cell locations.

2.7 Return flux in the entrance pupil

The photon flux returning from each LGS point source is considered uniformly distributed over the spherical surface of the wavefront. Since the solid angle Ω at which the telescope is seen from the source is typically very small, the variation of r^{free}_{lip} in the denominator of Eq. (2.5.2) over the pupil can be neglected. Thus, the fraction of energy emitting from a point source that passes through the telescope entrance pupil is

$$\frac{\Omega}{4\pi} = \frac{1}{4\pi} \frac{A_p}{|\boldsymbol{r}^t_{li}|^2 \cos^2 \beta^t_{li}}, \tag{2.7.1}$$

where A_p is the pupil area, $|\boldsymbol{r}^t_{li}|$ is the distance from pupil center to the point source, β^t_{li} is the angle between the telescope optical axis and the direction to the point source as seen from the pupil center,

$$\cos \beta^t_{li} = \left(\frac{\boldsymbol{r}^t_{li}}{|\boldsymbol{r}^t_{li}|} \right)_z. \tag{2.7.2}$$

The photon flux into the entrance pupil from a point source is

$$\Phi_{li} = \tau T_{AOS} \frac{T_{ATM}}{\cos \beta^g_{li}} s^{\mathtt{Na}} C^{\mathtt{Na}} P_l w_{li} \frac{\Omega}{4\pi},\ [\mathtt{photons}], \tag{2.7.3}$$

where

Exposure time	:	τ	$= 2$ ms,
Atmosphere transmittance	:	T_{ATM}	$= 0.89$,
AO system transmittance	:	T_{AOS}	$= 0.448$,
Sodium coupling efficiency	:	$s^{\mathtt{Na}}$	$= 130$ (photons m^2)/(s W atom),
Sodium abundance	:	$C^{\mathtt{Na}}$	$= 2.1 \times 10^{13}$ atoms/m^2,
Laser power per LGS	:	P_l	$= 20$ W,

β_{li}^{g} is the angle between zenith direction and the point source direction as viewed from the entrance pupil center.

The fluxes from all point sources are later summed on the detector.

3 Propagation through atmosphere

The goal of this section is to develop mathematical models that can deliver realistic intensity distributions on the Shack-Hartmann WFS taking into account:

1. the intensity distribution in the extended LGS light source formed by a specific laser launch telescope and distorted by the upward propagation through the turbulent atmosphere;
2. the phase distortion effects due to atmosphere on the downward light path from the LGS to the telescope;
3. the diffraction effects caused by the main and launch telescope apertures, WFS lenslets and the atmospheric turbulence;
4. anisoplanatic effects due to LGS extent;
5. scintillation effects due to the atmospheric turbulence.

3.1 Propagation geometry

The `Na` laser guide star is modeled as a set of point sources distributed within the `Na` layer and creating the extended light source shaped as a narrow column inclined with respect to the telescope line of sight and thus creating elongated images in the focal plane of the Shack-Hartmann WFS. The details of the LGS geometry are given in Section 2. Here we note that the point sources that make a LGS are incoherent and thus the intensity distribution on the detector is a sum of intensity distributions from each point source. This reduces the problem of elongated source propagation into a set of point source propagations, so in what follows we concentrate solely on the problem of the spherical wave propagation from a point source located at finite distance and shifted with respect to the telescope optical axis. Another assumption is a layered model for the atmospheric turbulence. Figure 2 shows the geometrical configuration used for the modeling. Note that we choose the turbulence layers orientation to be perpendicular to the telescope optical axis (see Sec. 2.5.1).

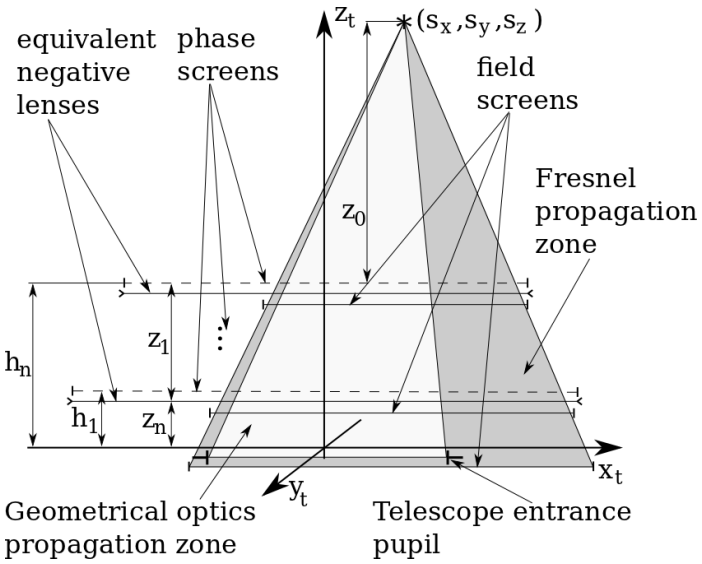

Figure 2: Geometry of point source propagation through atmosphere to the telescope entrance pupil. The orientation corresponds to the t-system, i.e. the z-axis is along the telescope optical axis.

Light from a point source with coordinates $\boldsymbol{s} = (s_x, s_y, s_z)$, and generally not on the telescope optical axis, propagates through random atmospheric turbulence phase screens located at altitudes $\{h_i\}_{i=1}^n$ that divide the whole path from the source to the telescope entrance pupil into a set of propagation paths $\{z_j\}_{j=0}^n$.

3.2 Geometrical optics propagation

Geometrical optics is a simple approximation that allows e.g. to derive the relationships between the statistics of the turbulence layers and the optical field on the sensors. The geometrical optics propagation is based on the following assumptions:

- Light is propagating along straight lines emerging from the point source and intersecting the telescope entrance pupil.
- Phase distortion along each ray is a sum of phase contributions from each phase screen at the point of intersection of the ray and the screen. From Figure 2 it is obvious that the coordinates (x, y) of the intersection point of ray and phase screen are

$$(x, y) = \frac{(s_z - h)}{s_z}((x_0, y_0) - (s_x, s_y)) + (s_x, s_y), \tag{3.2.1}$$

  where (x_0, y_0) are the coordinates of a point at the telescope entrance pupil, h is the phase screen altitude. Correspondingly, the phase deviation from the spherical wavefront at entrance pupil point (x_0, y_0) is

$$\phi(x_0, y_0) = \sum_{i=1}^{n} \phi(x, y)_i. \tag{3.2.2}$$

- Turbulence-induced intensity variations (scintillation) are neglected.
- Diffraction effects such as light scattering are not retrievable as the geometrical optics propagation is effectively just a scaled projection of the phase screens onto the entrance pupil.

Normally the phase screens are defined as maps of random phase values on a point grid. Thus, in order to find the phase at point $(x, y)_i$ some or other interpolation technique is needed. On a regular square grid the bilinear interpolation is the natural choice.

The geometrical optics propagation zone, i.e. the volume filled with rays that pass through the telescope entrance pupil, is shown on Figure 2 in light gray hatch. The minimal physical extent of a random phase map on each phase screen is defined by the point of intersection of the propagation zone with the phase screen such that this point is farthest from the telescope optical axis. Simple geometrical considerations lead to the estimate for the phase screen diameter

$$D_{ps} \geq \frac{(s_z - h)}{s_z}(D - 2(s_x^2 + s_y^2)_{max}^{1/2}) + 2(s_x^2 + s_y^2)_{max}^{1/2}, \tag{3.2.3}$$

where D is the telescope entrance pupil diameter and maximum is taken over all the point sources that make the LGS.

3.3 Generalized Fresnel propagation

The scalar diffraction using the Fresnel approximation is a more accurate propagation approach. Fresnel diffraction takes allows to estimate the scintillation and light scattering effects.

A complication of the diffraction propagation in case of the LGS is the necessity to effectively address divergence of the wavefronts. A brute force application of the classical Fresnel integral to the diverging spherical wave results in excessive sampling requirements. As an optimistic example, consider the optical field at the telescope entrance pupil from a pure spherical wave emitted by an on-axis point source located at altitude of 90 km. In parabolic approximation the optical field is

$$U(\boldsymbol{x}) = \exp(i\frac{k}{2z}|\boldsymbol{x}|^2),$$

where $k = 2\pi/\lambda$. The maximal local frequency defining the sampling is

$$f_{max} = \frac{1}{2\pi}\partial_x \left(\frac{k}{2z}|\boldsymbol{x}|^2\right)_{max}$$

is equal to $\frac{1}{3}\cdot 10^3$ m^{-1} for $\lambda = 0.5$ μm and telescope pupil diameter of 30 m. That is, the maximal sampling interval in the optical field maps is $\frac{1}{2f_{max}} = 1.5$ mm, much smaller that the interval needed to adequately sample the turbulence (≥ 1 cm). This results in unacceptably large $\sim 20K \times 20K$ optical field maps just to sample the oscillations in the spherical wave amplitude. To avoid this sampling issue the $\exp(i\frac{k}{2z}|\boldsymbol{x}|^2)$ factor needs to be somehow moved out of the diffraction integral. This can be done in the framework of the generalized Fresnel diffraction approach described in Appendix 9. Namely, a spherical wave propagation through a phase screen can be considered a plane wave propagation through a phase screen and a negative lens with focal distance equal to the curvature radius of the spherical wavefront at the screen. The propagation through the lens is governed by the Generalized Fresnel Transform (9.0.6) with the ABCD-matrix corresponding to the propagation through negative thin lens with focal distance f_1 followed by free propagation path of length z_1:

$$W = \begin{bmatrix} 1 & z_1 \\ 1/f_1 & 1 \end{bmatrix}. \tag{3.3.1}$$

Substituting W from Eq. (3.3.1) into the Cast-to-Convolution theorem or, equivalently, using first Focus and then Cast-to-convolution theorem, we find that after propagation through the phase screen-lens combination the diffracted field has the necessary factorized form

$$U(\boldsymbol{x}) = \exp(i\frac{k}{2f_2}|\boldsymbol{x}|^2)\tilde{U}(\boldsymbol{x}), \tag{3.3.2}$$

where $f_2 = f_1 + z_1$, $\tilde{U}(\boldsymbol{x})$ is a plane wave field 1) multiplied by the first phase screen, 2) Fresnel-propagated distance $z_1\frac{f_1}{z_1+f_1}$ to the next screen and 3) scaled by factor $\frac{f_1+z_1}{f_1}$ (see Eq. 9.0.8). Obviously, the next propagation step is identical to the first one after replacing z_1 with z_2 and f_1 with f_2, etc. Since the $\tilde{U}$-field is diffraction of the plane wave (multiplied by the turbulence random phase mask), the sampling requirements are significantly relaxed. Note that f_i in the parabolic phase factor $\exp(i\frac{k}{2f_i}|\boldsymbol{x}|^2)$ on each screen is equal just to the distance to the point source, i.e. represents the un-diffracted spherical wave complex amplitude on each screen; the scaling factor $\frac{f_i+z_i}{f_i}$ just shows how much the grid on ith screen expands when projected on $(i+1)$th screen along the rays emerging from the spherical wave center.

Some extra comments on the sampling are in order. A typical sampling requirement for the Fresnel propagation [9] is derived from the assumption that the range of propagation directions (and therefore the frequency range computed through the relationship $f_{max} = \alpha_{max}/\lambda$, where α_{max} is the maximum direction angle in the plane wave spectrum) is such that the entire phase screen is seen from any observation point. This results in

$$f_{max} \geq \frac{D}{\lambda z}, \tag{3.3.3}$$

where D is the screen (aperture) diameter, z is the propagation diestance. For a typical values for $D = 30$ m and $z = 2$ km, the $f_{max} \geq 3\cdot 10^4$ m^{-1}, which is way larger than the maximal resolved frequency of $\sim 10^2$ m^2 in the turbulence spectrum defined by the inverce of phase screen spacing, which is about 1 cm for the typical accumulated $r_0 = 20$ cm. Figure 3 is the illustration of the spectral extent for a typical turbulence phase screen, which suggests that the turbulence effectively works as a low-pass spatial filter with the bandwidth < 100 m^{-1}. Thus it is this bandwidth that defines the necessary sampling. Figure 4 illustrates that the frequency domain Fresnel propagation kernel is can also be sampled adequately within the frequency range of ~ 100 m^{-1}.

These observations allow to define a recursive algorithm for the diverging spherical wave diffraction by a sequence of turbulence phase screens. For more generality we assume that the propagation

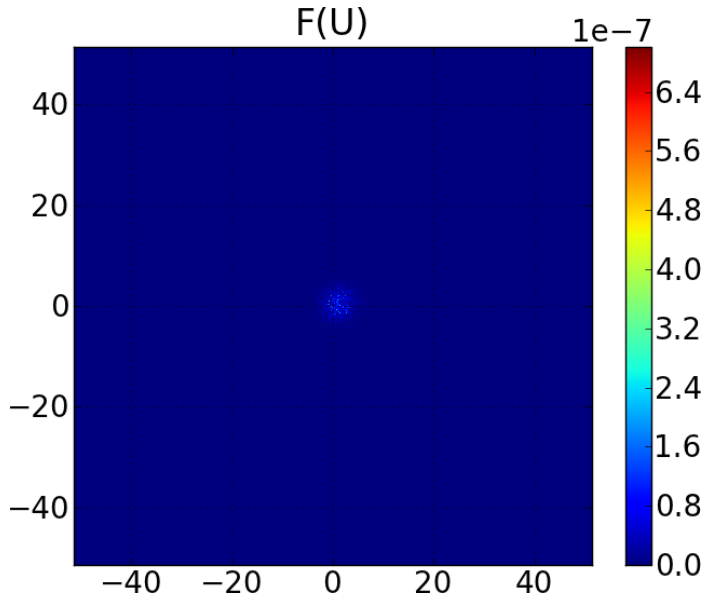

Figure 3: Typical spectrum amplitude of the ramdom phase screen with accumulated $r_0 = 20$ cm. XY-axes are spatial frequency, m^{-1}.

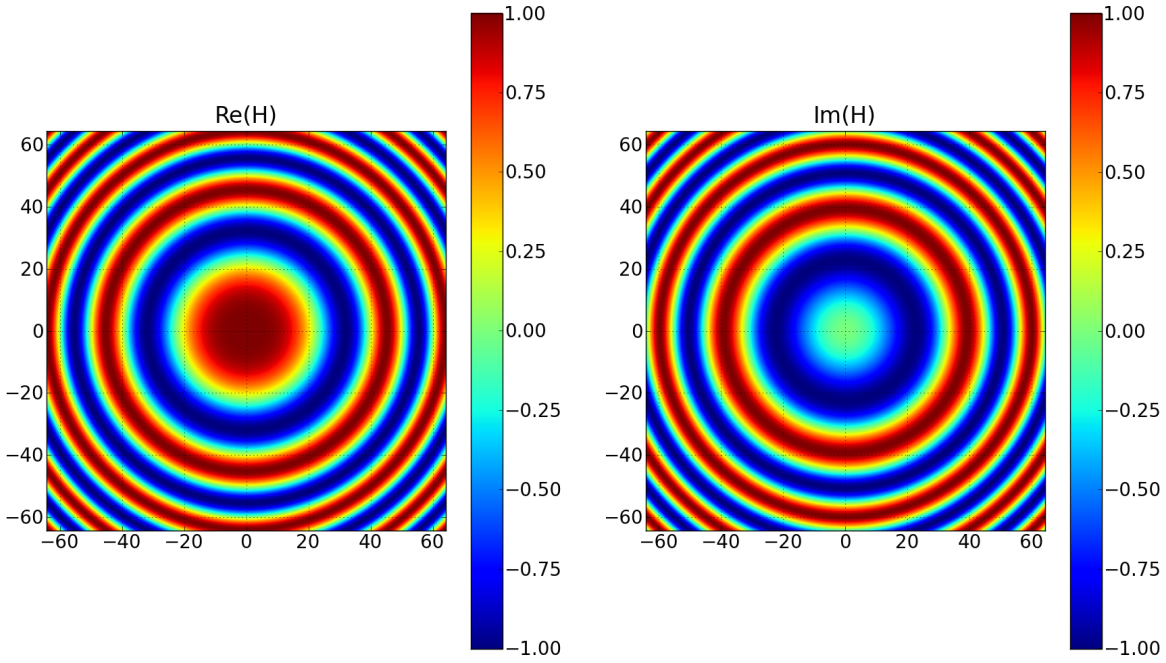

Figure 4: Maps for real and imaginary parts of the frequency domain Fresnel propagation kernel $H = \exp(-i\lambda z|f|^2)$ for $z = 2000$ m, $\lambda = 0.5$ μm. XY-axes are spatial frequency, m^{-1}.

from turbulent phase screen i to screen $i+1$ is not necessarily free-space but is governed by a non-trivial wave matrix W_i. We also need to take into account that propagation from multiple point sources making the LGS extended light source is done through the same turbulence volume, i.e. through the same set of phase screens. To take into account the shift of each point source with respect to the telescope optical axis it is best to perform propagation from this source in the shifted coordinate system in which the source is at $(0, 0, h_s)$ and to use interpolation to first read the phase values from the phase screen to the shifted field map and, in the end, to read the values from the propagated field map onto the entrance pupil grid. The following data/operation flow is assumed:

1. Preparational stage.

   - Define a set of the point sources making up a LGS: their $\{(s_x, s_y, s_z)_s\}_{s=1}^{\#PtS}$-coordinates and relative intensities (weights) $\{w_s\}_{s=1}^{\#PtS}$.
   - Set a working wavelength λ.
   - Define a turbulence model: number of turbulence layers, their altitudes $\{h_p\}_{p=1}^{\#PS}$, partial turbulence strengths via Fried parameters of C_n^2, inner and outer scales, etc.
   - Define a set of layer-to-layer propagation wave matrices $\{W_p\}_{p=1}^{\#PS}$. In case of free-space propagation between layers, the matrices are

     $$W_p = \begin{bmatrix} 1 & z_p \\ 0 & 1 \end{bmatrix}, \tag{3.3.4}$$

     where $\{z_p\}_{p=1}^{\#PS}$ are distances between layers, z_1 is the distance between last layer and the entrance pupil.
   - Generate a set $\{P_p\}_{p=1}^{\#PS}$ of the random phase screens on each turbulence layer. The key parameters for this operation are the physical size of each screen and its sampling interval dx_p. We note that, because of interpolation operation assumed to read from the phase screen into the optical field, the sampling of the screens does not have to be the same or equal to the optical field map sampling and can follow the natural sampling conditions on each screen

     $$dx_p = r_{0_p}/m, \ p = 1, ..., \#PS, \tag{3.3.5}$$

     where r_{0_p} is a partial Fried parameter for each screen, m-factor varies from 5 to 10. The physical size of each screen is determined by the "Fresnel propagation" zone shown on Figure 2. From the picture we see that the safe value for diameter D_p of a phase screen located at altitude h_p should be

     $$D_p \geq gD + 3(s_x^2 + s_y^2)_{max}^{1/2}, \tag{3.3.6}$$

     where D is the entrance pupil diameter, g is an oversize or "guard" factor ($g > 1$), h_0 is the point source altitude, and the maximum is taken over all the point sources.

2. Loop over point sources.

   - Find the focal distance of the equivalent negative lens on the first phase screen to propagate (which is the highest one!):

     $$f_{\#PS} = s_z - h_{\#PS}, \tag{3.3.7}$$

     where s_z is the z-coordinate (altitude) of the current point source.
   - Run the "propagation parameter recursion":

     $$\tilde{W}_p = W_p + \begin{bmatrix} B_p/f_p & 0 \\ D_p/f_p & 0 \end{bmatrix}, \tag{3.3.8}$$

     $$f_{p-1} = \frac{\tilde{A}_p}{\tilde{C}_p}, \ p = \#PS, ..., 1,$$

where W_p are the ABCD-matrices defined at the preparatory stage, $\tilde{W}_p$ are the "spherical wave propagation" ABCD-matrices formed according to Eqs. (9.0.12, 9.0.8). Note the descending layer counter. The $\{(\tilde{W}_p, f_p)\}_{p=1}^{\#PS}$-set completely defines parameters for spherical wave propagation through all the phase screens to the telescope entrance pupil by Eq. (9.0.8), f_0 defines the curvature of the spherical wave factor (see Eq. (3.3.2)) in the entrance pupil, the $\tilde{B}_p/\tilde{A}_p$ is the equivalent propagation distance from layer p to layer $p+1$, $\tilde{A}_p$ is the field grid expansion factor from layer p to $p+1$.

- Decide on the size and sampling interval for the field amplitude map to propagate. Generally, these parameters depend on the point source so this stage resides in the point source loop. We make the following observations:
  - In order to use FFT to evaluate the convolution in Eq. (9.0.8) the *pixel* size N of field map on each screen should be the same (otherwise an additional interpolation is needed). The physical size, however, is different on each screen, it is scaled by factor $\tilde{A}_p$. In the entrance pupil the physical field map size is

$$\tilde{D}_0 = \tilde{D}_{\#PS} \prod_{p=1}^{\#PS} \tilde{A}_p, \tag{3.3.9}$$

    where $\tilde{D}_{\#PS}$ is the diameter of the field map on the highest phase screen from where the propagation starts. According to Figure 2

$$\tilde{D}_0 \geq gD + (s_x^2 + s_y^2)_{max}^{1/2}. \tag{3.3.10}$$

  - Likewise, if the spacing on the highest field screen is decided to be equal to $dx_{\#PS}$, then the spacing on the same field screen propagated down to the entrance pupil will be

$$dx_0 = dx_{\#PS} \prod_{p=1}^{\#PS} \tilde{A}_p. \tag{3.3.11}$$

    Since $\tilde{A}_p \geq 1$, $\forall i$, for the most typical case of free-space propagation of the diverging spherical wave, $dx_0 \geq dx_{\#PS}$ but it is the last field screen that needs to be sampled the finest to represent the field distorted by the whole volume of the turbulence. So it would be wise to first choose dx_0 as a fraction of the Fried parameter r_0 for the whole turbulence volume then find $dx_{\#PS}$ on the first screen to propagate from Eq. (3.3.11).

  Thus, using Eq. (3.3.10) we decide on the field map physical size, choose dx_0, find the field map pixel size as

$$N = ceiling(\tilde{D}_0/dx_0) \tag{3.3.12}$$

  and find $dx_{\#PS}$ from Eq. (3.3.11) for the beginning of propagation sequence.

- Generate the Generalized Fresnel propagator maps $\{H_p\}_{p=1}^{\#PS}$. Note that this stage is sitting inside the point source loop because map spacings depend on the position of the current point source!

$$df_p = \frac{1}{N dx_p}, \tag{3.3.13}$$

$$\alpha_p = \frac{\tilde{A}_p}{\lambda \tilde{B}_p},$$

$$H_{p,mn} = \frac{i}{\alpha} \exp\left(-i\frac{\pi}{\alpha}((mdf_p)^2 + (mdf_p)^2)\right), \; i = \sqrt{-1},$$

$$dx_{p-1} = \tilde{A}_p dx_p,$$

$$p = \#PS, ..., 1, \;\; m, n = -N/2, ..., N/2.$$

  Factor i/α can be omitted. Note the descending layer counter.

- Perform actual propagation of $\tilde{U}$-field (see Eq. 3.3.2) down to the entrance pupil:

$$x_{mn} = (ndx_p + s_x)/dp_p, \tag{3.3.14}$$

$$y_{mn} = (mdx_p + s_y)/dp_p,$$

$$\tilde{U}_{mn} \leftarrow \tilde{U}_{mn} \exp\left[i\mathbb{B}(P_p, x_{mn}, y_{mn})\right],$$

$$\tilde{U} \leftarrow \mathbb{F}\left(\tilde{U}\right),$$

$$\tilde{U} \leftarrow \tilde{U} H_p,$$

$$\tilde{U} \leftarrow \mathbb{F}^{-1}\left(\tilde{U}\right),$$

$$p = \#PS, ..., 1, \;\; m, n = -N/2, ..., N/2,$$

  where $\leftarrow$ means "in-place" operation, $\mathbb{B}$ is the standard bilinear interpolation operator assuming that the map to interpolate *from* has unit spacing (other sort of interpolation can be used, of course), dp_p is the pth phase screen spacing, $\mathbb{F}$ is the Fourier transform operator.

- Interpolate the $\tilde{U}$-field defined on the shifted grid in the entrance pupil onto the another grid in the entrance pupil convenient for subsequent propagation through Shack-Hartmann WFS lenslets:

$$x_{mn} = (mdx - s_x + l_x)/dx_0, \tag{3.3.15}$$

$$y_{mn} = (ndx - s_y + l_y)/dx_0,$$

$$\tilde{G}_{mn} = \mathbb{B}(\tilde{U}, x_{mn}, y_{mn}),$$

$$m, n = -M/2, ..., M/2,$$

  where dx and M are the spacing and pixel size of the "lenslet map" grid, (l_x, l_y) is the lenslet map grid shift with respect to the pupil center. Then

$$G_{mn} = \exp\left[-i\frac{k}{2f_0}(x_{mn}^2 + y_{mn}^2)\right]\tilde{G}_{mn}, \tag{3.3.16}$$

$$x_{mn} = ndx - s_x + l_x, \;\; y_{mn} = mdx - s_y + l_y, \;\; m, n = -M/2, M/2.$$

  is the full field in the entrance pupil propagated from the current point source. This is the end of the propagation calculation for a single point source. Note that the last stage (the interpolation to lenslet map) can be omitted and attached to the next stage, the propagation through WFS lenslets. In this case the $\tilde{U}$-field is the final output of Fresnel propagation to the entrance pupil, which together with source xy-shift (s_x, s_y), pupil grid spacing dx_0 and the spherical wavefront equivalent focal distance f_0 are the outputs of this algorithm.

Figure 5 shows the cross section of the Monte-Carlo modeled coherence factor

$$\mu(r) = \frac{|\Gamma(r)|}{\Gamma(0)}, \tag{3.3.17}$$

where $\Gamma(r)$ is the propagated field auto-correlation function, compared to its theoretical value for the spherical wave

$$\mu(r) = \exp(-0.5D(r)), \tag{3.3.18}$$

$$D(r) = 2.91k^2 r^{5/3} \int_0^h (1 - \frac{z}{h}) C_{n^2}(z) dz,$$

where h is the propagation distance from the spherical wave center to the ground.

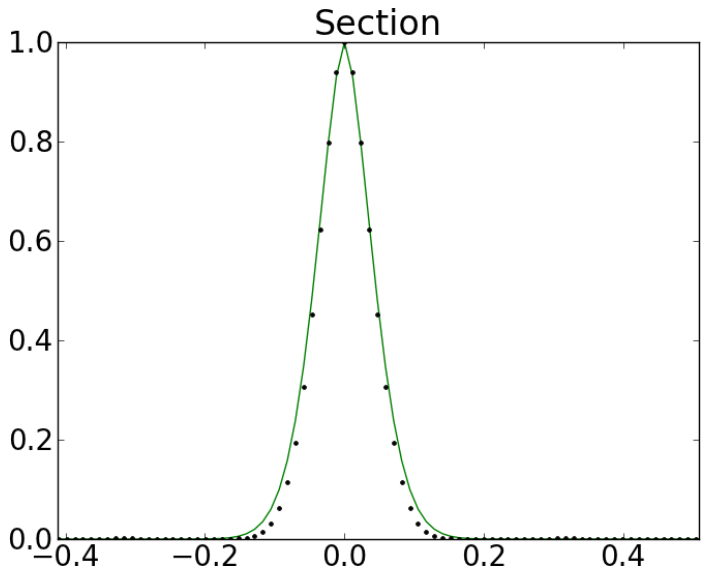

Figure 5: Theoretical (solid line) vs. numerical (dotted line) coherence factor cross-section for 10 layer propagation through Hufnagel-Valley turbulence profile. Propagation distance is 90 km, telescope diameter is 10 m, $\lambda = 0.5$ μm, 100 random trials averaged. X-axis units are meters of point separation.

4 Shack-Hartmann Wavefront sensor modeling

4.1 Nomenclature

$\boldsymbol{s} = (s_x, s_y)$ - vector of xy-slope measurements read from one Shack-Hartmann sensor subaperture, [m or pixels].

$I(x, y)$ - intensity distribution in the detector focal plane, [].

$\langle \boldsymbol{s}\boldsymbol{s}^T \rangle - \langle \boldsymbol{s} \rangle \langle \boldsymbol{s} \rangle^T$ - covariance matrix of the xy-slope measurements, [m^2 or pixel^2].

A - area of subaperture, [m^2].

p - detector pixel size, [m].

n_{ph} - number of photons passed through a subaperture, [].

σ_e - readout noise, [electrons/pixel].

f_L - lenslet focal distance, [m]

Γ_L - angular magnification in the detector exit pupil, [].

ε_{Na} - angular fwhm size of `Na` LGS projected to sky as seen from a subaperture, [rad].

ε_0 - angular fwhm size of a point source projected to sky as seen from a subaperture, [rad].

θ_e - orientation angle of the elongated spot on the detector, [rad].

4.2 Sensor geometry

TBD

4.3 Propagation from exit pupil to detector

The sampling of the pupil is derived from the sampling in the WFS detector focal plane. If n_d is the number of samples across each spot on the detector and the fwhm of the diffraction limited spot is sampled with k pixels, then the pupil sampling is $2Nn_d/k = Nn$, where N is number of subapertures across the pupil diameter, n is number of pixels across a subaperture diameter. It is required that either k or $1/k$ is an integer and that $k \leq 2$. It is worth nothing that a field stop the size of a subaperture field–of–view is assumed. The pixel scale and the field–of–view are given by λ/dk and $n_d\lambda/dk$, respectively, with λ the wavefront sensing wavelength and d the lenslet pitch.

The Shack–Hartmann wavefront sensor (SH–WFS) model

1. the telescope pupil Π is cut in $N \times N$ square pieces of $n \times n$ pixels corresponding to the $N \times N$ lenslet array, for the lenslet (k, l) this is

$$a_{kl} = \Pi[kn, \ldots, (k+1)n - 1][ln, \ldots, l(n+1) - 1] \quad k, l = 0, \ldots, N-1,$$

2. each square array is multiplied by a complex phase ramp to keep the spot at the center of the array in the free aberration case,

$$a'_{kl}(i, j) = a_{kl}(i, j) \exp(\iota\pi(i + j)(n - 1)/n') \quad i, j = 0, \ldots, n-1$$

   with $n' = 2n$ if n is even or $n' = 2n + 1$ if n is odd and $\iota = \sqrt{-1}$,

3. each square array is padded with zeros in both directions up to n',

$$a'_{kl}[n, \ldots, n' - 1][n, \ldots, n' - 1] = 0,$$

4. a discrete Fourier transform is performed on each zero–padded array,

$$\tilde{a}'_{kl} = DFT\left\{a'_{kl}\right\},$$

5. each resulting array is reduced to half its size,

$$\tilde{a}_{kl} = \tilde{a}'_{kl}[0, \ldots, n-1][0, \ldots, n-1],$$

6. the spot intensities are computed from the squared modulus of the reduced arrays,

$$b_{kl} = \left|\tilde{a}_{kl}\right|^2,$$

7. if needed i.e. $k < 2$, the intensity map are binned to the detector array size,

$$b'_{kl}(k, l) = \sum_{i=kn_d}^{(k+1)n_d-1} \sum_{j=ln_d}^{(l+1)n_d-1} b_{kl}(i, j) \quad k, l = 0, \ldots, n_d - 1$$

4.4 Centroiding methods

The four spot centroiding methods are considered for the GMT LTAO Shack-Hartmann sensors:

1. *Center of Gravity*:
$$\begin{bmatrix} s_x \\ s_y \end{bmatrix} = \frac{1}{\sum_{xy} I(x,y)} \sum_{xy} \begin{bmatrix} x \\ y \end{bmatrix} I(x,y), \tag{4.4.1}$$
where $\boldsymbol{s} = (s_x, s_y)$ is the slope readout from the spot, $I(x,y)$ is the intensity distribution read out from detector pixels, summation is done over the pixels in the area occupied by a single spot.

2. *Weighted Center of Gravity* is the Center of Gravity algorithm applied to image $I(x,y)I_0(x,y)$, where $I_0(x,y)$ is a *reference image*.

3. *Correlation* algorithm finds spot position as that of maximum of the correlation function
$$C(\boldsymbol{s}) = \sum_{xy} I(x,y) I_0(x - s_x, y - s_y), \tag{4.4.2}$$
where $I_0(x,y)$ is a reference image.

4. *Quad cell* centroiding algorithm is used in the tip/tilt WFS, which has 4 pixels per spot. The quad cell readout is
$$s_x = \frac{1}{\sum_{i=1}^{4} I_i}(I_1 + I_2 - I_3 - I_4), \tag{4.4.3}$$
$$s_y = \frac{1}{\sum_{i=1}^{4} I_i}(I_1 + I_3 - I_2 - I_4),$$
where $\{I_i\}_{i=1}^{4}$ are the four intensity reads from the quad cell pixels.

Discussion of these centroiding approaches is given in Ref. [1].

4.5 Sensor noise covariance matrix

This section describes the derivation of the noise covariance matrix for a SH–WFS with a $N_L \times N_L$ lenslet array paving a telescope pupil of diameter D. The spots of the SH–WFS are assumed to be seeing limited i.e. $r_0 < D/N_L$, r_0 is the Fried parameter. Thus, the projected to sky angular size of the spot formed by a lenslet is $\varepsilon_0 = \lambda/r_0$, λ is the WFS operational wavelength. The spot elongation due to elongated LGS is characterized by the $(\varepsilon_{Na}, \theta_e)$-pair of the fwhm angular size along the `Na` LGS elongation direction and the elongation orientation angle. Both these parameters depend on the mutual orientation lenslet and the LLT, altitude and thickness of the `Na` layer, and the LLT pointing. The calculation of the $(\varepsilon_{Na}, \theta_e)$-pair is described in Section 2.3.

The spot intensity profile due to the LGS is assumed to be Gaussian with elliptical cross section and the long ellipse axis is rotated by angle θ_e with respect to the camera focal plane xy-coordinates:

$$I_S(x,y) = \frac{n_{ph}}{2\pi\sigma_x\sigma_y} \exp\left(-\frac{x'^2 + y'^2}{2\sigma_x\sigma_y}\right), \tag{4.5.1}$$

where subscript S stands for the star image distribution, n_{ph} is the photon flux through the sub-aperture,

$$x' = x\cos(\theta_e) - y\sin(\theta_e), \tag{4.5.2}$$
$$y' = x\sin(\theta_e) + y\cos(\theta_e), \tag{4.5.3}$$

σ_x and σ_y are related to the fwhm of the non-elongated and elongated spot, respectively, as

$$\varepsilon_{x,y} = 2\sqrt{2\ln(2)}\sigma_{x,y}, \tag{4.5.4}$$
$$\varepsilon_{x,y} = f_L \Gamma_L \varepsilon_{0,Na}, \tag{4.5.5}$$

where f_L is the lenslet focal distance, Γ_L is the angular magnification in the exit pupil where the lenslet array is located.

The spot centroid xy-readout in the lenslet focal plane in case of the *Center of Gravity* centroiding algorithm is given by

$$\boldsymbol{s} = \begin{bmatrix} s_x \\ s_y \end{bmatrix} = \frac{1}{\iint_A I(x,y)\mathrm{d}x\mathrm{d}y} \iint_A \begin{bmatrix} x \\ y \end{bmatrix} I(x,y)\mathrm{d}x\mathrm{d}y, \tag{4.5.6}$$

where $I(x,y)$ is the complete intensity distribution in the spot that includes the star intensity disribution and some other additions, $A = (D/N_L)^2$ is the lenslet area.

4.6 Spot intensity distribution

To proceed with computation of the spot readout covariance assumptions about the spot intensity distribution need to be made:

1. The whole intensity distribution is

$$I(x,y) = I_S(x,y) + I_B(x,y), \tag{4.6.1}$$

   where $I_S(x,y)$ is given in Eq. (4.5.1), $I_e(x,y)$ is the background image due to sensor readout noise.

2. $I_S(x,y)$ and $I_B(x,y)$ are statistically independent, i.e. $\langle I_S(x,y) I_B(x,y)\rangle = 0$.

3. $\langle I_B(x,y)\rangle = 0$.

4. All the $I_S(x,y)$ distribution energy is concentrated inside region A, so $\iint_A I_S(x,y)\mathrm{d}x\mathrm{d}y \approx n_{ph} = const$.

5. The random process $I_B(x,y)$ is ergodic, so $0 = \langle I_B(x,y)\rangle \approx \iint_A I_B(x,y)\mathrm{d}x\mathrm{d}y$, which, together with the previous assumption gives $\iint_A I(x,y)\mathrm{d}x\mathrm{d}y \approx n_{ph}$.

6. Spot cross-talk is negligible, so spots from different lenslets are statistically independent. Therefore, the full WFS readout covariance matrix is block diagonal with 2x2 blocks corresponding to each spot xy-slope covariance.

7. Pixel intensities are statistically independent, i.e. $\langle I(x,y) I(x',y')\rangle = 0$.

Eq. (4.5.6) due to assumptions 5, 6 simplifies to

$$\boldsymbol{s} = \frac{1}{n_{ph}} \iint_A \begin{bmatrix} x \\ y \end{bmatrix} I(x,y)\mathrm{d}x\mathrm{d}y. \tag{4.6.2}$$

The covariance of the spot centroid readouts is given by

$$\langle \boldsymbol{s}\boldsymbol{s}^T\rangle - \langle \boldsymbol{s}\rangle\langle \boldsymbol{s}^T\rangle \tag{4.6.3}$$

$$= \frac{1}{n_{ph}^2} \iint_A \iint_A \begin{bmatrix} x_1x_2 & x_1y_2 \\ y_1x_2 & y_1y_2 \end{bmatrix} (\langle I(x_1,y_1) I(x_2,y_2)\rangle - \langle I(x_1,y_1)\rangle\langle I(x_2,y_2)\rangle)\mathrm{d}x_1\mathrm{d}y_1\mathrm{d}x_2\mathrm{d}y_2.$$

Substututing Eq. (4.6.1) and using assumptions 2, 3, and 7 we simplify this equation to

$$\langle \boldsymbol{s}\boldsymbol{s}^T\rangle - \langle \boldsymbol{s}\rangle\langle \boldsymbol{s}^T\rangle \tag{4.6.4}$$

$$= \frac{1}{n_{ph}^2} \iint_A \begin{bmatrix} x^2 & xy \\ xy & y^2 \end{bmatrix} (\sigma_I^2(x,y) + \sigma_B^2) \mathrm{d}x\mathrm{d}y,$$

where

$$\sigma_S^2(x,y) = \langle I_S^2(x,y)\rangle - \langle I_S(x,y)\rangle^2,$$

is the variance distribution in the star intensity distribution,

$$\sigma_B^2 = \langle I_B^2(x,y)\rangle = const.$$

is the readout noise variance. Thus the sensor readout covariance has two terms that can be treated independently.

4.7 Photon noise

The photon noise follows a Poisson statistics distribution with variance $\sigma_S^2(x,y) = I_S(x,y)$. Thus the spot centroid readouts covariance in the case of the photon noise is given by

$$\langle \boldsymbol{s}\boldsymbol{s}^T\rangle_S - \langle \boldsymbol{s}\rangle_S \langle \boldsymbol{s}^T\rangle_S \tag{4.7.1}$$

$$= \frac{1}{n_{ph}^2} \iint_A \begin{bmatrix} x^2 & xy \\ xy & y^2 \end{bmatrix} I_S(x,y)\, \mathrm{d}x\mathrm{d}y,$$

where n_{ph} is the number of photons per subaperture, x and y are the coordinates in the focal plane, the intensity $I_S(x,y)$ in the focal plane given by Eq. (4.5.1).

Substutuing Eq.(4.5.1) into Eq. (4.7.1) and performing the integration leads to

$$\langle \boldsymbol{s}\boldsymbol{s}^T\rangle_S - \langle \boldsymbol{s}\rangle_S \langle \boldsymbol{s}^T\rangle_S \tag{4.7.2}$$

$$= \frac{1}{n_{ph}} \begin{bmatrix} \sigma_x^2 \cos^2\theta_e + \sigma_y^2 \sin^2\theta_e & (\sigma_x^2 - \sigma_y^2)\cos\theta_e \sin\theta_e \\ (\sigma_x^2 - \sigma_y^2)\cos\theta_e \sin\theta_e & \sigma_x^2 \sin^2\theta_e + \sigma_y^2 \cos^2\theta_e \end{bmatrix}$$

$$= \begin{bmatrix} \sigma_{xx}^2 & \sigma_{xy}^2 \\ \sigma_{xy}^2 & \sigma_{yy}^2 \end{bmatrix}.$$

From Eq.(4.7.2), it is obvious that covariance is null when the spots are oriented either along the x or y axis or if the fwhms of both x and y axis are the same.

4.8 Read-out noise

The read-out noise follows a zero-mean Gaussian distribution of variance $\sigma_B^2 = \sigma_e^2/p^2$, where σ_e^2 is the number of read noise electrons squared per pixel area p^2. Since $\sigma_B^2 = const.$ and, with assumption that A is a square lenslet, we have

$$\sigma_B^2 \iint_A xy \mathrm{d}x\mathrm{d}y = 0,$$

$$\iint_A x^2 \mathrm{d}x\mathrm{d}y = \iint_A y^2 \mathrm{d}x\mathrm{d}y.$$

Thus the readout noise covariance matrix is diagonal:

$$\langle \boldsymbol{s}\boldsymbol{s}^T\rangle_B = \begin{bmatrix} \sigma_{ron}^2 & 0 \\ 0 & \sigma_{ron}^2 \end{bmatrix}. \tag{4.8.1}$$

For a square lenslet of size $d = D/N_L$ we get

$$\sigma_{ron}^2 = \left(\frac{\sigma_e}{p n_{ph}}\right)^2 \int_{-d/2}^{d/2}\int_{-d/2}^{d/2} x^2 \mathrm{d}x\mathrm{d}y = \frac{1}{12}\left(\frac{d^2\sigma_e}{p n_{ph}}\right)^2 = \frac{N_d^2}{12}\left(\frac{D\sigma_e}{N_L n_{ph}}\right)^2, \tag{4.8.2}$$

N_d is the total number of pixels used for computing the centroids.

Finally, the sensor readout noise covariance matrix for one lenslet is a sum of covariance matrices for photon and readout noises:

$$\langle \boldsymbol{s}\boldsymbol{s}^T\rangle_{S+B} - \langle \boldsymbol{s}\rangle_{S+B}\langle \boldsymbol{s}^T\rangle_{S+B} = \begin{bmatrix} \sigma_{xx}^2 + \sigma_{ron}^2 & \sigma_{xy} \\ \sigma_{xy} & \sigma_{yy}^2 + \sigma_{ron}^2 \end{bmatrix}. \tag{4.8.3}$$

For the whole lenslet array, the noise covariance matrix is a block diagonal with these matrices on the diagonal.

5 Deformable mirror modeling

5.1 Nomenclature

TBD

5.2 Deformable mirror geometry

TBD

5.3 Linear model

5.4 Influence functions

TBD

5.5 Fitting error

TBD

5.6 Internal dynamics

TBD

6 Control

6.1 Linear system model and discretization

In our treatment of an AO system modeling we follow closely the "natural modeling" approach described in Refs. [2, 3]. To begin with, we consider the simplest case of a single-conjugate AO system, which is modeled through the following fundamental inputs.

1. A light source to be imaged with an AO system (the *target*) creates a continuous phase distribution $\phi_0(\boldsymbol{x})$ in the telescope entrance pupil, which is the accumulated phase distortion along the path from a light source to the telescope that includes atmospheric turbulence distortion. It is supposed that the autocorrelation function $\langle\phi_0(\boldsymbol{x}_1)\phi_0(\boldsymbol{x}_2)\rangle_\phi$ is known.

2. A set $\{f_i(\boldsymbol{x})\}_{i=1}^{\#ACT}$ ($\#ACT$ is the number of DM actuators) of the DM actuator influence functions projected as phase correction in the telescope entrance pupil. We will write these functions in vectorial form $\boldsymbol{f}(\boldsymbol{x})$. Note that, same as $\phi(\boldsymbol{x})$, these functions depend on the light source. The DM correction is assumed to be a linear combination of the influence functions:
$$\phi_{DM}(\boldsymbol{x}) = \sum_{i=1}^{\#ACT} c_i f_i(\boldsymbol{x}) \tag{6.1.1}$$
or
$$\phi_{DM}(\boldsymbol{x}) = \boldsymbol{f}^T(\boldsymbol{x})\boldsymbol{c},$$
where $\boldsymbol{c}$ is the vector of DM correction commands.

3. A wavefront sensor (WFS) accepts light from a *reference* source not in general coinciding with the target. WFS is modeled as a linear mapping of the reference wavefront $\phi x, y$ in the entrance pupil to a set of sensor measurements:
$$\boldsymbol{s} = \mathcal{M}[\phi(\boldsymbol{x})], \tag{6.1.2}$$
where $\mathcal{M}$ is a linear *measurement operator*. The *measurement equation* describing the full linear sensor model is
$$\boldsymbol{s} = \mathcal{M}[\phi(\boldsymbol{x}) + \delta\phi(\boldsymbol{x})] + \boldsymbol{n}, \tag{6.1.3}$$
where $\boldsymbol{n}$ is random sensor readout noise with known autocorrelation matrix $\langle\boldsymbol{n}\boldsymbol{n}^T\rangle_n$, $\delta\phi(\boldsymbol{x})$ is an additive aberration due to propagation from telescope entrance pupil to the exit pupil conjugate to the WFS location. We will assume for the moment that this aberration can be perfectly calibrated out, so $\delta\phi(\boldsymbol{x}) = 0$.

This small set of parameters are enough to fully describe a linear model of an AO system.

6.2 Minimum Mean Square Error AO control

The goal of the *Minimum Mean Square Error* (MMSE) AO control is to find a command vector $\hat{\boldsymbol{c}}$ such that the DM correction minimizes the target wavefront mean square phase error (*quadratic cost*) in the telescope entrance pupil
$$\langle J\rangle_{\phi,n} = \langle||\phi_0 - \phi_{DM}||^2\rangle_{\phi,n}, \tag{6.2.1}$$
where Hilbert space norm
$$||a(\boldsymbol{x})||^2 = [a(\boldsymbol{x}), a(\boldsymbol{x})] = \frac{1}{|A|}\int_A ds\, a^2(\boldsymbol{x}), \tag{6.2.2}$$
is derived from the Hilbert space metric
$$[a(\boldsymbol{x}), b(\boldsymbol{x})] = \frac{1}{|A|}\int_A ds\, a(\boldsymbol{x})b(\boldsymbol{x}), \tag{6.2.3}$$
A is the telescope entrance pupil domain (the *aperture*), $|A|$ is the aperture area, and $\langle\rangle_\phi$ denotes averaging over joint statistics of the input turbulent wavefront and the sensor noise. We can consider two cases of the quadratic cost minimization: 1) *DM fitting* and 2) *phase estimation*.

6.2.1 DM fitting

The DM fitting problem statement is: given target wavefront phase $\phi_0(\boldsymbol{x})$ at the entrance pupil find the DM command vector $\hat{\boldsymbol{c}}$ such that the deterministic wavefront error is minimized:

$$\hat{\boldsymbol{c}} = \arg\min_{\forall \boldsymbol{c}} ||\phi_0 - \boldsymbol{f}^T \boldsymbol{c}||^2. \tag{6.2.4}$$

It is known from the theory of Hilbert spaces that the above equation is equivalent to

$$[\phi_0 - \boldsymbol{f}^T \hat{\boldsymbol{c}}, \boldsymbol{f}] = 0, \tag{6.2.5}$$

which is a form of the *orthogonality principle* stating that

`the optimal fitting error is orthogonal to the subspace spanned by the influence functions.`

Solving Eq. (6.2.4) or the equivalent Eq. (6.2.5) yields for the optimal control command

$$\hat{\boldsymbol{c}} = [\boldsymbol{f}, \boldsymbol{f}^T]^\dagger [\boldsymbol{f}, \phi_0], \tag{6.2.6}$$

where $[\boldsymbol{f}, \boldsymbol{f}^T]$ is called *Gramm matrix* of the function set $\boldsymbol{f}(\boldsymbol{x})$, † stands for pseudo inverse. The Gramm matrix is square and is invertible in case the influence functions $\boldsymbol{f}(\boldsymbol{x})$ are linearly independent. Since linear independence is not guaranteed for the real DM influence functions, the filtered pseudo-inverse is used. Note that in case of pseudo-inverse the orthogonality principle does not hold exactly. This, however, is easily fixed if we redefine the influence functions as, e.g., a subset of orthogonal singular modes of the Gramm matrix with sufficiently large singular values.

The optimal *fitting error* is

$$\begin{aligned} J_c &= [\phi_0 - \boldsymbol{f}^T \hat{\boldsymbol{c}}, \phi_0 - \boldsymbol{f}^T \hat{\boldsymbol{c}}] \\ &= [\phi_0 - \boldsymbol{f}^T \hat{\boldsymbol{c}}, \phi_0] \\ &= [\phi_0, \phi_0] - [\boldsymbol{f}^T, \phi_0][\boldsymbol{f}, \boldsymbol{f}^T]^\dagger [\boldsymbol{f}, \phi_0], \end{aligned} \tag{6.2.7}$$

where we used Eqs. (6.2.5) and (6.2.6). The orthogonality principle states that the phase can be presented as a sum of two mutually orthogonal *controllable* $\hat{\phi}_0$ and *uncontrollable* $\check{\phi}_0$ parts

$$\phi(\boldsymbol{x}) = \hat{\phi}_0(\boldsymbol{x}) + \check{\phi}_0(\boldsymbol{x}), \tag{6.2.8}$$

where

$$\hat{\phi}_0 = \boldsymbol{f}^T [\boldsymbol{f}, \boldsymbol{f}^T]^\dagger [\boldsymbol{f}, \phi_0] = \mathcal{F}\phi_0, \tag{6.2.9}$$

$$\check{\phi}_0 = \phi_0 - \mathcal{F}(\phi_0) = (\mathcal{I} - \mathcal{F})\phi_0 \tag{6.2.10}$$

and $\mathcal{F}, \mathcal{I} - \mathcal{F}$ are orthogonal projection operators on, respectively, *controllable* and *uncontrollable subspaces* of the influence function set $\boldsymbol{f}$. Note that the dimension of the controllable subspace is finite, so either $\hat{\boldsymbol{c}}$ or $\boldsymbol{\phi}_0 = [\boldsymbol{f}, \phi_0]$ are the natural discrete representations for the controllable part of the wavefront phase, the only part of interest in the AO control.

6.2.2 Phase estimation

The phase estimation problem statement is: given sensor measurements $\boldsymbol{s}$ find an estimate $\tilde{\phi}_0(\boldsymbol{x})$ of the target source phase in the entrance pupil such that the mean square error is minimized over the measurement statistics, in our case, the joint turbulence and sensor noise statistics:

$$\tilde{\phi}_0 = \arg\min_{\forall \mathcal{E}} \langle ||\phi_0 - \mathcal{E}\boldsymbol{s}||^2 \rangle_{\phi,n}, \tag{6.2.11}$$

where $\mathcal{E}$ is the linear estimator operator. Analogously to the deterministic orthogonality principle the *orthogonality principle of statistical estimation* states that

`optimal estimator error is statistically orthogonal to the measurements,`

i.e., for our case

$$\langle(\mathcal{E}\boldsymbol{s}-\phi_0)\boldsymbol{s}^T\rangle_{\phi,n}=0. \tag{6.2.12}$$

Solving Eq. (6.2.11) or its equivalent (6.2.12) yields

$$\tilde{\phi}_0=\langle\phi_0\boldsymbol{s}^T\rangle_{\phi,n}\langle\boldsymbol{s}\boldsymbol{s}^T\rangle^{-1}_{\phi,n}\boldsymbol{s}. \tag{6.2.13}$$

The optimal estimation error is

$$\begin{aligned}\langle J_e\rangle_{\phi,n}&=\langle[\phi_0-\tilde{\phi}_0,\phi_0-\tilde{\phi}_0]\rangle_{\phi,n} \\ &=\langle[\phi_0-\tilde{\phi}_0,\phi]\rangle_{\phi,n} \\ &=\langle[\phi_0,\phi_0]\rangle_{\phi,n}-\langle\phi_0\boldsymbol{s}^T\rangle_{\phi,n}\langle\boldsymbol{s}\boldsymbol{s}^T\rangle^{-1}_{\phi,n}\langle\boldsymbol{s}\phi_0\rangle_{\phi,n},\end{aligned} \tag{6.2.14}$$

where Eqs. (6.2.12), (6.2.13) were used.

Comparison Eq. (6.2.13) with Eq. (6.2.9) reveals the fact that the statistical estimation and fitting problems have essentially the same structure. Indeed, Eq. (6.2.13) coincides with Eq. (6.2.9) for the controllable part of the wavefront after substitutions

$$\begin{aligned}\langle\boldsymbol{s}\phi_0(\boldsymbol{x})\rangle_{\phi,n}&\to\boldsymbol{f}(\boldsymbol{x}),\ \texttt{(estimation influence functions)},\\ \langle\boldsymbol{s}\boldsymbol{s}^T\rangle_{\phi,n}&\to[\boldsymbol{f},\boldsymbol{f}^T],\ \texttt{(estimation Gramm matrix)},\\ \boldsymbol{s}&\to[\boldsymbol{f},\phi_0],\ \texttt{(projection on measurements)},\\ \tilde{\phi}_0&\to\hat{\phi}_0,\ \texttt{(observable part of wavefront)}.\end{aligned}$$

Thus, there exists another, "observable-unobservable", orthogonal decomposition of the input wavefront (see Ref. [3] for the proof):

$$\phi_0(\boldsymbol{x})=\tilde{\phi}_0(\boldsymbol{x})+\bar{\phi}_0(\boldsymbol{x}), \tag{6.2.15}$$

where

$$\tilde{\phi}_0=\langle\boldsymbol{s}^T\phi_0\rangle_{\phi,n}\langle\boldsymbol{s}\boldsymbol{s}^T\rangle^{-1}_{\phi,n}\mathcal{M}\phi=\mathcal{O}\phi, \tag{6.2.16}$$

$$\bar{\phi}_0=\phi_0-\mathcal{O}\phi. \tag{6.2.17}$$

Again, the observable part of the wavefront, the only part of interest for AO wavefront sensing, is finite-dimensional, and either $\boldsymbol{s}$ or $\boldsymbol{w}=\langle\boldsymbol{s}\boldsymbol{s}^T\rangle^{-1}_{\phi,n}\boldsymbol{s}$ can be naturally used as discrete representations of the $\tilde{\phi}_0$.

6.2.3 Joint estimation and fitting, separation principle

Now consider the problem of joint estimation and fitting, namely, given measurement $\boldsymbol{s}$ and a set of influence functions $\boldsymbol{f}(\boldsymbol{x})$ find the control commands $\hat{\boldsymbol{c}}$ such that

$$\hat{\boldsymbol{c}}=\mathcal{C}\boldsymbol{s}=\arg\min_{\forall\mathcal{C}}\langle||\phi_0-\boldsymbol{f}^T\mathcal{C}\boldsymbol{s}||^2\rangle_{\phi,n}, \tag{6.2.18}$$

where $\mathcal{C}$ is the estimator matrix creating linear mapping from the set of sensor measurements to the set of DM commands. Expanding the norm in Eq. (6.2.18) one gets

$$\begin{aligned}||\phi_0-\hat{\phi}||^2&=||(\phi_0-\tilde{\phi}_0)+(\tilde{\phi}_0-\hat{\phi})||^2 \\ &=||\bar{\phi}_0||^2+2[\bar{\phi}_0,\tilde{\phi}_0-\boldsymbol{f}^T\mathcal{C}\boldsymbol{s}]+||\tilde{\phi}_0-\boldsymbol{f}^T\mathcal{C}\boldsymbol{s}||^2, \\ \hat{\phi}&=\boldsymbol{f}^T\mathcal{C}\boldsymbol{s}.\end{aligned} \tag{6.2.19}$$

$\langle[\bar{\phi}_0,\tilde{\phi}_0-\boldsymbol{f}^T\mathcal{C}\boldsymbol{s}]\rangle_{\phi,n}=0$ for an optimal phase estimate $\tilde{\phi}_0$ because of the orthogonality principle (6.2.12). Thus

$$\begin{aligned}\langle J\rangle_{\phi,n}&=\langle||\phi-\hat{\phi}||^2\rangle_{\phi,n} \\ &=\langle||\bar{\phi}_0||^2\rangle_{\phi,n}+\langle||\tilde{\phi}_0-\boldsymbol{f}^T\mathcal{C}\boldsymbol{s}||^2\rangle_{\phi,n},\end{aligned} \tag{6.2.20}$$

which is known as the *separation principle of the quadratic control*. Eq. (6.2.20) shows that the overall error can be minimized in two independent steps:

1. Find the observable part of the target phase $\tilde{\phi}_0$ from Eq. (6.2.13).
2. Since $\tilde{\phi}_0$ is not a stochastic quantity, the $\langle\rangle_{\phi,n}$ brackets can be dropped for the second term reducing its minimization to deterministic fitting of the actuator influence functions to the phase estimate according to Eq. (6.2.6).

Following this path, i.e. substituting Eq. (6.2.13) into Eq. (6.2.6), we get for the optimal reconstructor matrix

$$\hat{\mathcal{C}} = [\boldsymbol{f}, \boldsymbol{f}^T]^\dagger [\boldsymbol{f}, \langle \phi_0 \boldsymbol{s}^T \rangle_{\phi,n}] \langle \boldsymbol{s}\boldsymbol{s}^T \rangle_{\phi,n}^{-1}. \tag{6.2.21}$$

The error for this reconstructor is

$$\langle \hat{J} \rangle_{\phi,n} = \langle \bar{\phi}_0 \rangle_{\phi,n} + \langle \breve{\bar{\phi}}_0 \rangle_{\phi,n}, \tag{6.2.22}$$

where the first term is the phase estimation error given by Eq. (6.2.14), second term is the fitting error of the observable phase to the influence functions and is given by Eq. (6.2.7) after substituting $\tilde{\phi}_0$ instead of ϕ_0.

Another important result derived in Ref. [3] concerns with the estimate of the reconstruction error due to non-optimal reconstruction matrix:

$$\langle J \rangle_{\phi,n} - \langle \hat{J} \rangle_{\phi,n} = \mathtt{Tr} \left\{ [\boldsymbol{f}, \boldsymbol{f}^T](\mathcal{C} - \hat{\mathcal{C}}) \langle \boldsymbol{s}\boldsymbol{s}^T \rangle_{\phi,n} (\mathcal{C} - \hat{\mathcal{C}})^T \right\}, \tag{6.2.23}$$

where $\mathcal{C}$ is the arbitrary control matrix that is not computed according to prescription (6.2.21) and $\langle J \rangle_{\phi,n}$ is the corresponding reconstruction error.

6.2.4 Estimator for projected wavefront

A modification of the phase estimation algorithm is needed for the situation when it is necessary to find an estimate of the input phase part extractable from $\phi(\boldsymbol{x})$ by a projection operation

$$\phi_p(\boldsymbol{x}) = \mathcal{P}(\phi_0(\boldsymbol{x})), \tag{6.2.24}$$

where $\mathcal{P}$ is a linear *projection operator*. Examples of such an operator are the controllable/uncontrollable $\mathcal{F}, (\mathcal{I} - \mathcal{F})$ projectors discussed above, the high-pass and low-pass spatial filters that are an indispensable part of the GMT LTAO control strategy to be discussed later in this document.

The optimal minimum least squares estimator for $\mathcal{P}(\phi_0)$ wavefront instead of ϕ_0 is derived from the minimization problem

$$\mathcal{E}_p = \arg\min_{\forall \mathcal{E}} \langle |\mathcal{P}(\phi_0) - \mathcal{E}\boldsymbol{s}|^2 \rangle \tag{6.2.25}$$

or from the orthogonality principle

$$\langle (\mathcal{P}(\phi_0) - \mathcal{E}_p \boldsymbol{s}) \boldsymbol{s}^T \rangle = 0, \tag{6.2.26}$$

which, due to linearity of $\mathcal{P}$, trivially yealds

$$\mathcal{E}_p = \mathcal{P}(\mathcal{E}), \tag{6.2.27}$$

where $\mathcal{E}$ is given by Eq. (6.2.13). Interesting, if Eq. (6.2.27) is used to find an optimal estimate of the controllable part $\hat{\phi}_0$ of the input phase, Eq. (6.2.21) for the optimal joint reconstructor results.

6.2.5 Information deficiency in the WFS model. Aliasing error.

Practical MMSE controllers prove to be sub-optimal due to information deficiency in the underlying system models. The MMSE approach is model-based, i.e. it relies on the internal mathematical representation of the real system. It is the ultimate goal of the system modeling for the MMSE-based AO control to build the internal model only on physically measurable (calibratable) data. There are, however, multiple causes for the necessary data to be un-measurable. A fundamental model

deficiency is that only finite-dimensional approximation of the sensor measurement operator $\mathcal{M}$ is possible based on the measurable data because this operator maps the infinite-dimensional space $\mathbb{H}$ of the wavefront phases $\phi(\boldsymbol{x})$ onto finite-dimensional space $\mathbb{S}$ of the sensor readouts. Assume there are orthogonal bases in both $\mathbb{H}$ and $\mathbb{S}$. Since the dimensionality of the $\mathbb{H}$-basis is higher than that of $\mathbb{S}$ there is no way to find such a pair of bases that each $\mathbb{S}$ basis function maps onto exactly one $\mathbb{H}$ basis function, i.e. generally all components of $\phi(\boldsymbol{x})$, low and high order, act on ("alias with") each WFS measurement s_i. The aliasing is not a problem as long as the $\mathcal{M}$ operator is known exactly because in this case the $\langle \phi_0 \boldsymbol{s}^T \rangle$ and $\langle \boldsymbol{s}\boldsymbol{s}^T \rangle$ catch the correct "aliasing pattern". One can, however, practically measure only $\mathcal{M}(\mathcal{P}\phi)$, where $\mathcal{P}$ is the projector on a finite-dimensional subspace of $\mathbb{H}$. The resulting finite-dimensional measurement operator $\mathcal{M}\mathcal{P}$, if substituted into Eq. (6.1.3) and then into Eq. (6.2.21) will result in not quite correct aliasing pattern prediction and thus in a suboptimal reconstructor. The corresponding additional *aliasing error* can be estimated through Eq. (6.2.23) once exact or at least more elaborated model for the true measurement operator $\mathcal{M}$ is known.

A natural choice for the finite dimensional measurement operator approximation $\mathcal{M}\mathcal{P}$ is when $\mathcal{P} = \mathcal{F}$, the projection on the controllable subspace (see Eq. (6.2.9)). In this case $\mathcal{M}\mathcal{P} = \mathcal{M}\boldsymbol{f}^T = \mathcal{D}$, where $\mathcal{D}$ is the DM *poke matrix* that is measurable by recording sensor readouts due to action of a DM actuator controlled ("poked") one at a time. Since, generally, the controllable part of the wavefront reliably represents low spacial frequency content of the wavefront aberrations, it is wise to apply low-pass spatial filter to the reference wavefront ϕ falling on the sensor in order to reduce the discrepancy between the true action $\mathcal{M}(\mathcal{P}_{LP}\phi)$ of the low-pass filtered wavefront and its prediction $\mathcal{M}\mathcal{P}(\mathcal{P}_{LP}\phi)$ and thus the aliasing error [5]. Note that the optimal reconstructor equation (6.2.21) has to be modified by replacing $\boldsymbol{s} = \mathcal{M}\phi$ with $\boldsymbol{s}_{LP} = \mathcal{M}(\mathcal{P}_{LP}\phi)$, which, in general, will increase the optimal reconstruction error. This increase is, however, expected to be compensated with the much more significant decrease of the aliasing error contribution.

6.2.6 Dynamic and closed-loop control

The MMSE controller described above is an oversimplified version of a real AO control algorithm based on two fundamental simplifying assumptions:

- *Open-loop operation*: it is assumed that the sensor measures input signal in the exit pupil directly, without any correction elements in the optical path in front of the sensor. A real AO system rarely works in open-loop regime because of small dynamic range of the existing WFSs. The more practical *closed-loop* operation assumes that all the correction elements (DMs, tip/tilt mirrors, etc.) are located in front of sensors and the latter measure the difference between the input signal (turbulent wavefront) and its correction by DMs. In this case the input to the WFS is not $\phi(\boldsymbol{x})$ but $\delta\phi(\boldsymbol{x})$ and the input to controller is not $\boldsymbol{s}$ but $\delta\boldsymbol{s}$, the *error signal*.

- *Non-dynamic* operation: it is assumed that signals propagate through the control system instantaneously and without temporal shape distortions. In reality, dynamic effects exist in the system. Two most important of them are: 1) signal delays due to data transfers, CCD exposure/readout time and controller computation time, 2) signal distortions due to finite temporal bandwidth of the correction mechanism actuators. The dynamic effects increase the residual error and may also lead to system instability in closed-loop regime. To introduce dynamic effects one has to consider all quantities to be time-dependent by adding n sub-index, $n = 1, ..., \infty$, for discrete time.

Simplified signal block diagrams for an AO system in open-loop and closed-loop configurations are shown on Fig. 6. The system dynamics are modeled by adding: 1) k-step signal delay element with z-domain transfer function z^{-k} to account for delays in sensor and controller; 2) a filter with z-domain transfer function (matrix) $d(z)$ to account for the DM dynamic effects. It is possible to derive a relationship between the open-loop (or *feedforward*) reconstructor $\mathcal{C}$ and the closed-loop (or *feedback*) one $\mathcal{C}_{FB}$ by noticing that, to deliver the same output signal, it should be

$$\mathcal{C}\boldsymbol{s} = \mathcal{C}_{FB}\delta\boldsymbol{s}. \tag{6.2.28}$$

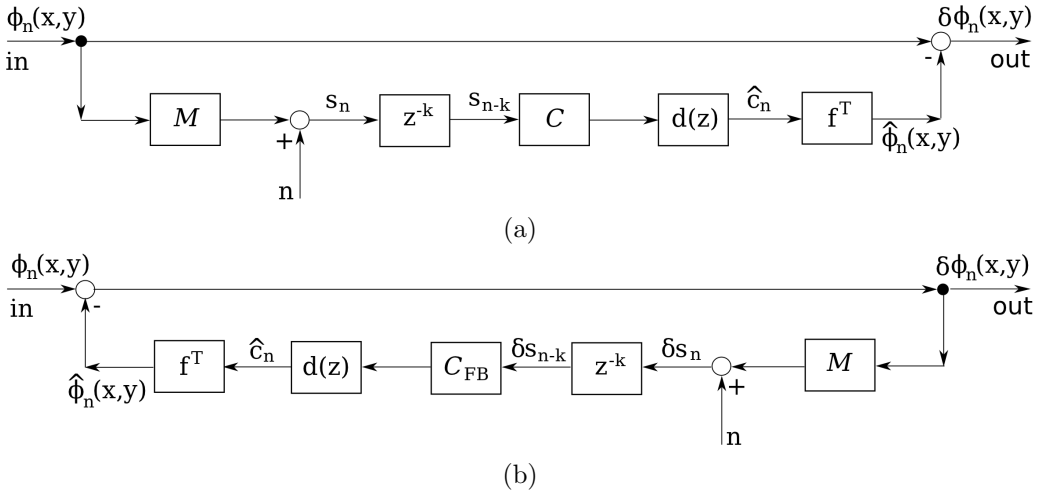

Figure 6: Open-loop (a) and closed-loop (b) AO controller block diagrams.

From the diagrams:

$$\delta \boldsymbol{s}(z) = \boldsymbol{s}(z) - z^{-k} d(z) \mathcal{M}(\boldsymbol{f}^T \mathcal{C}_{FB} \delta \boldsymbol{s}(z)) \tag{6.2.29}$$

$$= \boldsymbol{s}(z) - z^{-k} d(z) \mathcal{D} \mathcal{C}_{FB} \delta \boldsymbol{s}(z),$$

where $\mathcal{D} = \mathcal{M}(\boldsymbol{f}^T)$ is the *poke matrix* relating action of each DM influence function on the WFS measurements. Substitution of Eq. (6.2.29) into Eq. (6.2.28) yields

$$\mathcal{C}_{FB} = \mathcal{C}(\mathcal{I} - z^{-1} d(z) \mathcal{C}\mathcal{D})^{-1}. \tag{6.2.30}$$

The transfers from input wavefront phase $\phi(n)$ to the AO system residual phase error $\delta\phi(n)$ (*error rejection transfer function*): for the feedforward and feedback controllers shown on Fig. 6 are:

$$(\phi \to \delta\phi)(z) = \mathcal{I} - z^{-k} d(z) \mathcal{D}\mathcal{C}; \tag{6.2.31}$$

$$(\phi \to \delta\phi)_{FB}(z) = (\mathcal{I} + z^{-k} d(z) \mathcal{D}\mathcal{C}_{FB})^{-1}. \tag{6.2.32}$$

The open-loop reconstructor $\mathcal{C}$ can also be used directly in the *pseudo open-loop* (POL) setting of the closed-loop control when the open-loop measurement is approximately restored through an internal model for the DM. In the case of linear internal model the approximate (pseudo) open-loop WFS measurement $\hat{\boldsymbol{s}}$ is

$$\hat{\boldsymbol{s}} = \delta \boldsymbol{s} + \mathcal{D} \boldsymbol{c}. \tag{6.2.33}$$

Block diagram for a dynamic MMSE controller working in the POL regime is shown on Fig. 7. The integrator/corrector filter $g(z)$ is used to produce the absolute DM commands from differential ones in a way ensuring system stability and dynamic error minimization.

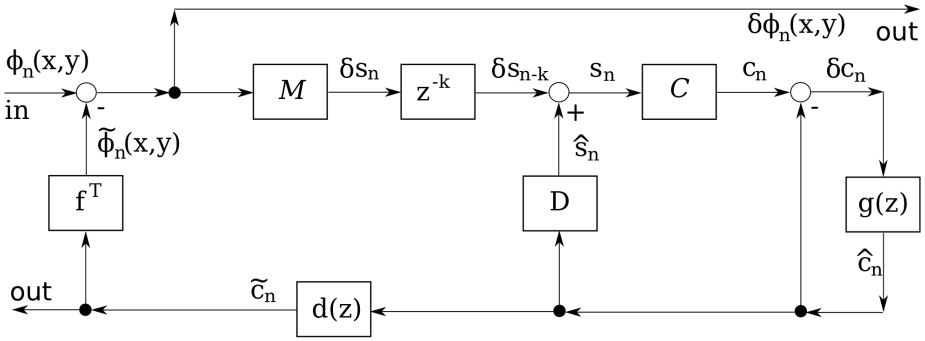

Figure 7: Pseudo Open-Loop MMSE controller block diagram.

The set of dynamic equations for the POL controller is:

(pseudo open-loop measurement)

$$\boldsymbol{s}(n) = \delta\boldsymbol{s}(n-k) + \hat{\boldsymbol{s}}(n); \tag{6.2.34}$$

(pseudo open-loop command)

$$\boldsymbol{c}(n) = \mathcal{C}\boldsymbol{s}(n); \tag{6.2.35}$$

(command increment)

$$\delta\boldsymbol{c} = \boldsymbol{c}(n) - \hat{\boldsymbol{c}}(n); \tag{6.2.36}$$

(integrator/corrector state space equations, see Appendix 8)

$$\boldsymbol{x}^g(i+1) = \mathcal{A}^g\boldsymbol{x}^g(n) + \mathcal{B}^g\delta\boldsymbol{c}(n), \tag{6.2.37}$$

$$\hat{\boldsymbol{c}}(n) = \mathcal{C}^g\boldsymbol{x}^g(n) + \mathcal{D}^g\delta\boldsymbol{c}(n); \tag{6.2.38}$$

(pseudo open-loop measurement estimate)

$$\hat{\boldsymbol{s}}(n) = \mathcal{D}\hat{\boldsymbol{c}}(n). \tag{6.2.39}$$

Two important transfer functions (matrices) can be derived from the Fig. 7 diagram: 1) the transfer from WFS output $\delta\boldsymbol{s}(n)$ to controller output $\hat{\boldsymbol{c}}(n)$ (*controller transfer function*):

$$(\delta\boldsymbol{s} \to \hat{\boldsymbol{c}})_{POL}(z) = z^{-2}g(z)\left[\mathcal{I} + g(z)(\mathcal{I} - \mathcal{R}\mathcal{D})\right]^{-1}\mathcal{C}, \tag{6.2.40}$$

and 2) the error rejection transfer function:

$$(\phi \to \delta\phi)_{POL}(z) = \left[\mathcal{I} + d(z)\boldsymbol{f}^T(\delta\boldsymbol{s} \to \hat{\boldsymbol{c}})_{POL}(z)\mathcal{D}\right]^{-1}. \tag{6.2.41}$$

Being formally equivalent, feedforward, feedback and POL controllers have different stability and error propagation properties.

6.3 Tomographic MMSE reconstructor

A generalization of the single-conjugate AO control is the *star-oriented tomography*. The AO control problem is restated as:

- Given is a set of thin phase screens (PS) $\{\phi^t_{PS}(\boldsymbol{x})\}^{\#PS}_{t=1}$ located at a number of altitudes above the telescope and representing the atmospheric turbulence on the path from a light sources to the telescope aperture.
- Likewise, given is a set of phase screens $\{\phi^m_{DM}(\boldsymbol{x})\}^{\#DM}_{m=1}$ representing the corrections by several DMs that are conjugated to a number of altitudes above the telescope. Each DM phase screen is a linear combination of the DM influence functions:

$$\phi^m_{DM}(\boldsymbol{x}) = \boldsymbol{f}_m(\boldsymbol{x})\boldsymbol{c}_m, \tag{6.3.1}$$

where $\boldsymbol{f}_m(\boldsymbol{x})$ are the m^{th} DM influence function set, $\boldsymbol{c}_m$ is the m^{th} DM control command vector.

- There are $\#TAR$ scientific targets to be imaged. Associated with each target and each PS or DM is a set $(\{\mathcal{T}_{lt}^{PS}\}_{l=1,t=1}^{\#TAR,\#PS}, \{\mathcal{T}_{lm}^{DM}\}_{l=1,m=1}^{\#TAR,\#DM})$ of the *propagation operators* that map PS or DM phase distributions to the wavefront phase distribution in the telescope entrance pupil. With assumption that these operators are linear, which is justified for weak turbulence, the phase from l^{th} light source in the entrance pupil due to all PS phase distortions and all DM phase corrections is

$$\delta\phi_0^l(\boldsymbol{x}) = \sum_{t=1}^{\#PS} \mathcal{T}_{lt}^{PS}(\phi_{PS}^t(\boldsymbol{x})) - \sum_{m=1}^{\#DM} \mathcal{T}_{lm}^{DM}(\phi_{DM}^m(\boldsymbol{x})),\ l = 1, ..., \#TAR. \tag{6.3.2}$$

- Likewise, there are $\#REF$ reference sources feeding light to wavefront sensors conjugated to the telescope entrance pupil. Associated with the reference sources as well as the PSs and DMs are the propagation operators $(\{\mathcal{R}_{st}^{PS}\}_{s=1,t=1}^{\#REF,\#PS}, \{\mathcal{R}_{sm}^{DM}\}_{s=1,m=1}^{\#REF,\#DM})$ mapping PS or DM phase distributions to the wavefront phase distribution in the sensor conjugate exit pupils. The closed-loop phase distribution on an s^{th} sensor due to all PS phase distortions and all DM phase corrections is

$$\delta\phi^s(\boldsymbol{x}) = \sum_{t=1}^{\#PS} \mathcal{R}_{st}^{PS}(\phi_{PS}^t(\boldsymbol{x})) - \sum_{m=1}^{\#DM} \mathcal{R}_{sm}^{DM}(\phi_{DM}^t(\boldsymbol{x})),\ s = 1, ..., \#REF. \tag{6.3.3}$$

  Correspondingly, the s^{th} sensor (closed-loop) readouts are

$$\delta\boldsymbol{s}_s = \mathcal{M}_s(\delta\phi^s(\boldsymbol{x})), \tag{6.3.4}$$

  where $\mathcal{M}_s$ is the measurement opertor associated with s^{th} sensor.

- The goal of the tomographic AO control is: given a set of sensor measurements $\boldsymbol{s} = \{\boldsymbol{s}_s\}_{s=1}^{\#REF}$ find the commands on all the DMs such that to minimize

$$\langle J\rangle_{\phi,n} = \sum_{l=1}^{\#TAR} w_l \langle ||\delta\phi_0^l||^2 \,|\, \boldsymbol{s}\rangle_{\phi,n}, \quad \sum_{l=1}^{\#TAR} w_l = 1, \tag{6.3.5}$$

  where $\boldsymbol{w} = \{w_l\}_{l=1}^{\#TAR}$ is the set of *target direction relative weights* and the conditional expectation (estimator) is taken over the joint statistics of the turbulence layers and the sensor noise.

For compactness of notation we introduce the following concatenations:

- Propagation operator matrices

$$\mathcal{T}^{PS} = \{\mathcal{T}_{lt}^{PS}\}_{l=1,t=1}^{\#TAR,\#PS}; \tag{6.3.6}$$

$$\mathcal{T}^{DM} = \{\mathcal{T}_{lm}^{DM}\}_{l=1,m=1}^{\#TAR,\#DM}; \tag{6.3.7}$$

$$\mathcal{R}^{PS} = \{\mathcal{R}_{st}^{PS}\}_{s=1,t=1}^{\#REF,\#PS}; \tag{6.3.8}$$

$$\mathcal{R}^{DM} = \{\mathcal{R}_{sm}^{DM}\}_{s=1,m=1}^{\#REF,\#DM}. \tag{6.3.9}$$

- Phase vectors

$$\boldsymbol{\phi}_{PS}(\boldsymbol{x}) = \{\phi_{PS}^t(\boldsymbol{x})\}_{t=1}^{\#PS}; \tag{6.3.10}$$

$$\boldsymbol{\phi}_{DM}(\boldsymbol{x}) = \{\phi_{DM}^m(\boldsymbol{x})\}_{m=1}^{\#DM}; \tag{6.3.11}$$

$$\delta\boldsymbol{\phi}_0(\boldsymbol{x}) = \{\delta\phi_0^l(\boldsymbol{x})\}_{l=1}^{\#TAR}; \tag{6.3.12}$$

$$\delta\boldsymbol{\phi}(\boldsymbol{x}) = \{\delta\phi^s(\boldsymbol{x})\}_{s=1}^{\#REF}. \tag{6.3.13}$$

- Sensor measurement vector
$$\delta \boldsymbol{s} = \{\mathcal{M}_s(\delta\phi^s(\boldsymbol{x}))\}_{s=1}^{\#REF}. \tag{6.3.14}$$

- DM influence matrix and control command vector
$$\mathcal{F}(\boldsymbol{x}) = \mathtt{diag}\{\boldsymbol{f}_m(\boldsymbol{x})\}_{m=1}^{\#DM}; \tag{6.3.15}$$
$$\boldsymbol{c} = \{\boldsymbol{c}_m\}_{m=1}^{\#DM}. \tag{6.3.16}$$

- Target direction weighting matrix
$$\mathcal{W} = \mathtt{diag}\{w_l\}_{l=1}^{\#TAR}, \tag{6.3.17}$$
and the *weighted norm*
$$||\boldsymbol{\phi}||^2_{\mathcal{W}} = \sum_i w_i ||\boldsymbol{\phi}_i||^2 = [\boldsymbol{\phi}^T, \mathcal{W}\boldsymbol{\phi}]. \tag{6.3.18}$$

In this notation the minimization problem for the cost function given in Eq. (6.3.5) can be written as
$$\hat{\boldsymbol{c}} = \arg\min_{\forall \boldsymbol{c}} \langle ||\mathcal{T}^{PS}(\boldsymbol{\phi}_{PS}) - \mathcal{T}^{DM}(\mathcal{F}^T)\boldsymbol{c}||^2_{\mathcal{W}} \mid \boldsymbol{s}\rangle_{\phi,n}, \tag{6.3.19}$$
which is a tomographic analog of Eq. (6.2.18).

The tomographic analog to the deterministic DM fitting problem is then stated as: find the control commands $\hat{\boldsymbol{c}}$ for all DMs such that
$$\hat{\boldsymbol{c}} = \arg\min_{\forall \boldsymbol{c}} ||\mathcal{T}^{PS}(\boldsymbol{\phi}_{PS}) - \mathcal{T}^{DM}(\mathcal{F}^T)\boldsymbol{c}||^2_{\mathcal{W}}. \tag{6.3.20}$$

To derive solution to this problem we first consider the matrix analog to the orthogonality principle Eq. (6.2.5). Replace each influence function $f_i(\boldsymbol{x})$ with e.g. a finite vector of its values on the entrance pupil point grid:
$$f_i(\boldsymbol{x}) \to \boldsymbol{f}_i = \{f_i(\boldsymbol{x}_j)\}_{j=1,\#PT},\ i = 1, ..., \#ACT.$$
Then $\boldsymbol{f}^T(\boldsymbol{x})\boldsymbol{c} \to \mathcal{F}^T\boldsymbol{c}$, where $\mathcal{F}^T = [\boldsymbol{f}_1 ... \boldsymbol{f}_{\#ACT}]$ and the matrix form of Eq. (6.2.5) reads as
$$\mathcal{F}(\boldsymbol{x}_0 - \mathcal{F}^T\boldsymbol{c}) = 0,\ \boldsymbol{x}_0 = \{\phi_0(\boldsymbol{x}_j)\}_j^{\#PT}. \tag{6.3.21}$$
Applying this to Eq. (6.3.20) one derives by analogy
$$[(\mathcal{T}^{DM}(\mathcal{F}^T))^T, \mathcal{T}^{PS}(\boldsymbol{\phi}_{PS}) - \mathcal{T}^{DM}(\mathcal{F}^T)\boldsymbol{c})]_{\mathcal{W}} = 0 \tag{6.3.22}$$
and
$$\hat{\boldsymbol{c}} = [(\mathcal{T}^{DM}(\mathcal{F}^T))^T, \mathcal{T}^{DM}(\mathcal{F}^T)]^{-1}_{\mathcal{W}} [(\mathcal{T}^{DM}(\mathcal{F}^T))^T, \mathcal{T}^{PS}(\boldsymbol{\phi}_{PS})]_{\mathcal{W}}, \tag{6.3.23}$$
where the *weighted Hilbert metric* is defined as
$$[\boldsymbol{a}(\boldsymbol{x}), \boldsymbol{b}(\boldsymbol{x})]_{\mathcal{W}} = [\boldsymbol{a}^T(\boldsymbol{x}), \mathcal{W}\boldsymbol{b}(\boldsymbol{x})], \tag{6.3.24}$$
$[*, *]$ is the usual Hilbert space metric. Correspondingly, the controllable part of the phase in the entrance pupil for all the target directions is
$$\hat{\boldsymbol{\phi}}_0 = \mathcal{T}^{DM}(\mathcal{F}^T)\hat{\boldsymbol{c}}. \tag{6.3.25}$$

The tomographic phase estimation problem is stated as: find the estimate of phase $\tilde{\boldsymbol{\phi}}_0$ in entrance pupil for all the target directions such that
$$\tilde{\boldsymbol{\phi}}_0 = \arg\min_{\forall \mathcal{E}} \langle ||\mathcal{T}^{PS}(\boldsymbol{\phi}_{PS}) - \mathcal{E}\boldsymbol{s}||^2_{\mathcal{W}}\rangle_{\phi,n} \tag{6.3.26}$$

with the solution written by analogy with Eq. (6.2.13)

$$\tilde{\boldsymbol{\phi}}_0 = \langle \mathcal{T}^{PS}(\boldsymbol{\phi}_{PS})\boldsymbol{s}^T\rangle_{\phi,n}\langle \boldsymbol{s}\boldsymbol{s}^T\rangle^{-1}_{\phi,n}\boldsymbol{s}. \tag{6.3.27}$$

Finally, according to the separation principle, the tomographic reconstructor generates the estimate $\hat{\tilde{\boldsymbol{\phi}}}_0$ optimal in the sense of Eq. (6.3.19) by substitution of Eq. (6.3.27) into Eq. (6.3.23) and then into Eq. (6.3.25). This completes the description of a general tomographic star-oriented AO system.

The GMT LTAO system can be described as a group of inter-connected tomographic AO sub-systems. The detailed mapping of the AO control theory developed in the previous sections onto the GMT LTAO is given in the next section.

6.4 GMT LTAO sub-systems

According to the *split control concept* the entire GMT LTAO system can be viewed as a set of weakly interacting control sub-systems (feedback loops, see Fig. 4-35 in Ref. [6]):

1. The *ASM high order LGS-based* (ASM HO LGS) control loop intended to reject high spatial order atmospheric/telescope aberrations and using the LGS return for WFS measurements. This channel has the following features:
   - This channel works in closed-loop behind ASM.
   - Target is ϕ_{Sc} is the wavefront from a scientific object.
   - Reference is ϕ_{LGS} is the wavefront from 6 LGSs.
   - The control commands generated in this channel are sent to the ASM.
   - The wavefront sensors for this channel are the 6 LGS WFSs.
   - The sampling rate is the one of the LGS WFSs.
2. The *ASM low order NGS-based* (ASM LO NGS) or "truth" control loop is used to provide low order ASM correction, which is impossible to determine from the LGSs. Another possible use of the LO NGS WFS is to sense the primary segment differential pistons. This channel has the following features:
   - This channel works in closed-loop behind ASM and OI DM.
   - Target is the wavefront ϕ_{Sc} from a scientific object.
   - Reference is the wavefront ϕ_{NGS} from one NGS.
   - The control commands generated by this channel are sent to ASM.
   - The wavefront sensor for this channel is the LO NGS WFS ("truth sensor").
   - The sampling rate is the one of the LO NGS WFS.
3. The *ASM tip/tilt NGS-based* (ASM TT NGS) control loop intended to sense and correct the waveront tip/tilt in the scientific object direction using a natural guide star. This channel has the following features:
   - This channel works in closed-loop behind ASM and OI DM.
   - Target is the wavefront ϕ_{Sc} from a scientific object.
   - Reference is the wavefront ϕ_{NGS} from one NGS.
   - The control commands generated in this channel are sent to the ASM.
   - The wavefront sensor for this channel is a quad-cell tip/tilt NGS (TT NGS) WFS.
   - The sampling rate is the one of the TT WFS.

4. The *OI DM high order LGS-based* (OI DM HO LGS) control loop is for correcting the NGS wavefront by the OI DM in order to improve performance of the NGS TT channel. This channel has the following features:

   - This channel works in closed-loop behind ASM.
   - Target is the wavefront ϕ_{NGS} from a NGS.
   - Reference is the wavefront ϕ_{LGS} from 6 LGSs.
   - The control commands generated in this channel are sent to OI DM.
   - The wavefront sensors for this channel are the 6 LGS WFSs.
   - The control algorithm is closed-loop with respect to the ASM but open-loop with respect to OI DM.
   - The sampling rate is the one of the LGS WFSs.

5. The *OI DM low order NGS-based* (OI DM LO NGS) control loop is to provide the low order OI DM correction, which is not possible to determine from the LGSs. This channel has the following features:

   - This channel works in closed-loop behind ASM and OI DM.
   - Target is the wavefront ϕ_{NGS} from a NGS.
   - Reference is the wavefront ϕ_{NGS} from the same NGS.
   - The control commands generated by this channel are sent to OI DM.
   - The wavefront sensor for this channel is the LO NGS WFS.
   - The sampling rate is the one of the LO NGS WFS.

One has also to mention some auxiliary control channels used for or together with LTAO. They are not based on the standard AO control and use other control approaches.

1. *LGS focus stabilization subsystem* is used for adjusting the LGS WFS module focal plane to follow slow LGS position changes in the sky. This channel has the following features:

   - The feedback signal is the global focus mode extracted from the 6 LGS WFS measurements.
   - The control is applied to a servo actuator moving the whole LGS WFS module to adjust to the focus. The controller needs to be optimized to the (actuator + LGS module) dynamics.

2. *LGS pupil de-rotation subsystem* is used for compensation of the exit pupil rotation on the LGS module induced by changes in the telescope pointing. This channel has the following features:

   - The feedback signal for this channel is the correlated part of the LGS WFS spot motions.
   - The control is applied to a servo actuator rotating the whole LGS WFS module to adjust to the pupil rotation.

3. *OI WFS acquisition/image stabilization subsystem* is used find the NGS in the telescope field-of-view, to point the light from an NGS to the OI WFS detectors and stabilize it. This channel has the following features:

   - An acquisition camera is used to provide a signal to the controller.
   - The control is applied to a two degree-of-freedom actuator attached to the acquisition flat mirror located inside OI WFS module.
   - The acquisition camera and mirror work in closed-loop regime behind ASM and OI DM.

4. *GMT phasing subsystem* is an *active optics* system that keeps the telescope aligned, phased and shape-stabilized.

The auxiliary control sub-systems do not directly participate in the AO correction but the errors in these systems become the additional error inputs for the main AO controllers thus upsetting indirectly the AO system performance.

6.5 GMT LTAO models

This section describes elements of the GMT LTAO system mathematical description: signals, commands, matrices, operators, transfer functions.

6.5.1 LTAO system element models

GMT LTAO system is a version of the star-oriented tomographic controller with several channels as described in the previous section. The main physical parts of the system that need to be modeled together with their interaction are:

1. Six (6) Laser Launch Telescopes (LLT) generating six off-axis, finite-altitude `Na` Laser Guide Stars (LGS) in regular pattern in the sky. The LGS geometry is described in detail in Sec. 2. Table 1 gives approximate (subject to change in the course of development) parameters of the GMT LGS reference light sources.

	1	2	3	4	5	6
x_l^t, m						
y_l^t, m						
z_l^t, m						
α_l^t, rad						
β_l^t, rad						
$h_{\mathtt{Na}}$, m	90×10^3					

Table 1: GMT LGS parameters: $(x, y, z)_l^t$ – l^{th} LLT location coordinates with respect to GMT entrance pupil; $(\alpha, \beta)_l^t$ – l^{th} LLT direction (first and second Euler angles) with respect to GMT optical axis; $h_{\mathtt{Na}}$ – mean altitude of the `Na` layer. See Sec. 2 for details about the notation.

2. One (1) infinite-altitude Natural Guide Star (NGS) for tip/tilt and possibly other low order aberration sensing. It can be located anywhere within $2''$ telescope field of view. Note that the NGS is a reference source for the LGS channel and also both target and reference source for the On-Instrument WFS channel.

3. One infinite-altitude (1) Science Target (ST) light source to be imaged through LTAO system. Normally it is assumed to be on the GMT optical axis but we reserve a possibility for it to be at $(\alpha, \beta)_{ST}^t \neq 0$ off-axis direction (first and second Euler angles) with respect to the optical axis.

4. Atmospheric turbulence propagation path. It is parameterized by the C_n^2 profile, wind profile, split in to a number of discrete turbulence phase screens (PS) located at altitudes $\{h_s\}_{s=1}^{\#PS}$, with the covariance functions $\{\langle \phi_s^{PS}(\boldsymbol{x}_1, \boldsymbol{x}_2) \rangle\}_{s=1}^{\#PS}$, where $\boldsymbol{\phi}^{PS}(\boldsymbol{x}) = \{\phi_s^{PS}(\boldsymbol{x})\}_{s=1}^{\#PS}$ are the instantaneous phase distributions on the screens (see details in Section 1). Propagation from the target and reference light sources through the atmosphere is described through the propagation operator matrices:

   - $\mathcal{T}_{ST}^{PS}$ – propagates light from the scientific target through turbulence phase screen phase distributions $\boldsymbol{\phi}^{PS}(\boldsymbol{x})$ to the entrance pupil.

- $\mathcal{R}^{PS}_{LGS}$ – propagates light from the 6 LGSs through turbulence phase screen phase distributions $\boldsymbol{\phi}^{PS}(\boldsymbol{x})$ to the entrance pupil.
- $\mathcal{R}^{PS}_{NGS}$ – propagates light from the NGS through turbulence phase screen phase distributions $\boldsymbol{\phi}^{PS}(\boldsymbol{x})$ to the entrance pupil.

5. GMT entrance pupil. It is parameterized through:
   - Pupil location $(x, y, z)^g_t$ and orientation $(\alpha, \beta)^g_t$ coordinates with respect to the laboratory coordinate system (see Sec. 2). The
   - Pupil shape (see Ref. [7]).
6. GMT deformable mirrors:
   - Adaptive Secondary Mirror (ASM). It is parameterized by the set of influence functions $\boldsymbol{f}_{ASM}$ and DM phase screen $\phi_{DM}(\boldsymbol{x})$ conjugated to altitude $h_{ASM} = TBD$ and the ASM transfer matrix $\mathcal{H}_{ASM}(z)$ responsible for the mirror dynamics.
   - Analogously, the On-Instrument Deformable Mirror (OI DM) is parameterized through $\boldsymbol{f}_{DM}$, $\phi_{DM}(\boldsymbol{x})$, $h_{DM} = TBD$, $\mathcal{H}_{DM}(z)$.

   Light propagation from the target and reference sources through ASM and DM phase screens to the entrance pupil is described by propagation operator matrices:
   - $\mathcal{T}^{DM}_{ST}$ – propagates light from the scientific target through OI DM to the entrance pupil.
   - $\mathcal{T}^{ASM}_{ST}$ – propagates light from the scientific target through ASM to the entrance pupil.
   - $\mathcal{R}^{ASM}_{LGS}$ – propagates light from the 6 LGSs through ASM to the entrance pupil.
   - $\mathcal{R}^{DM}_{NGS}$ – propagates light from the NGS through OI DM to the entrance pupil.
   - $\mathcal{R}^{ASM}_{NGS}$ – propagates light from the NGS through ASM to the entrance pupil.

   More details on the GMT deformable mirrors can be found in Sec. 5.
7. There are three (3) wavefront sensors:
   - LGS HO WFS consisting of 6 sensor blocks. It is described by poke matrix $\mathcal{D}^{ASM}_{LGS}$ for interaction between LGS HO WFS and ASM, sensor noise covariance matrix $\langle \boldsymbol{n}_{LGS} \boldsymbol{n}^T_{LGS} \rangle$, anti-aliasing filter operator $\mathcal{P}_{LGS}$ for action of the LGS HO WFS field stops on the input wavefront phase.
   - NGS TT WFS described by matrix $\mathcal{D}^{ASM}_{TT}$ describing interaction between NGS TT WFS and ASM, poke matrix $\mathcal{D}^{DM}_{TT}$ for interaction between NGS TT WFS and the OI DM, sensor noise covariance matrix $\langle \boldsymbol{n}_{TT} \boldsymbol{n}^T_{TT} \rangle$, anti-aliasing filter operator $\mathcal{P}_{TT}$ describing action of the NGS TT WFS field stop on the input wavefront phase.
   - NGS LO WFS described by matrix $\mathcal{D}^{ASM}_{LO}$ for interaction between NGS TT WFS and ASM, poke matrix $\mathcal{D}^{DM}_{LO}$ for interaction between NGS LO WFS and the OI DM, sensor noise covariance matrix $\langle \boldsymbol{n}_{LO} \boldsymbol{n}^T_{LO} \rangle$, anti-aliasing filter operator $\mathcal{P}_{LO}$ describing action of the NGS LO WFS field stop on the input wavefront phase.

   More details on the GMT wavefront sensors can be found in Sec. 4.
8. The following signals circulate in the system:
   - $\boldsymbol{\phi}_{PS}(\boldsymbol{x})$ – instantaneous phase distortions on the atmospheric turbulence phase screens.
   - $\boldsymbol{\phi}_{ASM}(\boldsymbol{x})$ – instantaneous phase corrections on the ASM.
   - $\boldsymbol{\phi}_{DM}(\boldsymbol{x})$ – instantaneous phase corrections on the OI DM.
   - $\delta\boldsymbol{\phi}^{HO}_{ST}(\boldsymbol{x}) = \mathcal{T}^{PS}_{ST}(\boldsymbol{\phi}_{PS}) - \mathcal{T}^{ASM}_{ST}(\boldsymbol{\phi}_{ASM})$ – instantaneous phase distribution in the entrance pupil from atmospheric turbulence and ASM corrections propagated from the Science Target. This is the scientific target wavefront seen in the LGS HO WFS channel and, up to non-common path aberrations, in the scientific instrument channel.

- $\delta\boldsymbol{\phi}^{OI}_{ST}(\boldsymbol{x}) = \mathcal{T}^{PS}_{ST}(\boldsymbol{\phi}_{PS}) - \mathcal{T}^{ASM}_{ST}(\boldsymbol{\phi}_{ASM}) - \mathcal{T}^{DM}_{ST}(\boldsymbol{\phi}_{DM})$ – instantaneous phase distribution in the entrance pupil from atmospheric turbulence and both ASM and OI DM corrections propagated from the Science Target. This is the scientific target wavefront seen in the OI WFS channel.
- $\delta\boldsymbol{\phi}^{HO}_{LGS}(\boldsymbol{x}) = \mathcal{R}^{PS}_{LGS}(\boldsymbol{\phi}_{PS}) - \mathcal{R}^{ASM}_{LGS}(\boldsymbol{\phi}_{ASM})$ – instantaneous phase distribution in the entrance pupil from both atmospheric turbulence and DM corrections propagated from the 6 LGSs. This is the reference source wavefront(s) seen in the LGS HO WFS channel.
- $\delta\boldsymbol{\phi}^{HO}_{NGS}(\boldsymbol{x}) = \mathcal{R}^{PS}_{NGS}(\boldsymbol{\phi}_{PS}) - \mathcal{R}^{ASM}_{NGS}(\boldsymbol{\phi}_{ASM})$ – instantaneous phase distribution in the entrance pupil from atmospheric turbulence and ASM corrections propagated from the Science Target. This is the NGS wavefront seen in the LGS HO WFS channel and used as a target for the OI DM control algorithm.
- $\delta\boldsymbol{\phi}^{OI}_{NGS}(\boldsymbol{x}) = \mathcal{R}^{PS}_{NGS}(\boldsymbol{\phi}_{PS}) - \mathcal{R}^{ASM}_{NGS}(\boldsymbol{\phi}_{ASM}) - \mathcal{R}^{DM}_{NGS}(\boldsymbol{\phi}_{DM})$ – instantaneous phase distribution in the entrance pupil from atmospheric turbulence and both ASM and DM corrections propagated from the NGS. This is the reference source wavefront seen in the OI WFS channel.
- $\delta\boldsymbol{s}_{LGS} = \mathcal{M}^{LGS}\mathcal{P}_{LGS}(\delta\boldsymbol{\phi}^{HO}_{LGS}) + \boldsymbol{n}_{LGS}$ – instantaneous LGS HO WFS readout, where $\mathcal{M}_{LGS}$ is exact (infinite-dimensional) LGS HO WFS measurement operator, $\boldsymbol{n}_{LGS}$ is the instantaneous LGS HO WFS noise readout.
- $\delta\boldsymbol{s}_{TT} = \mathcal{M}^{TT}\mathcal{P}_{TT}(\delta\boldsymbol{\phi}^{OI}_{NGS}) + \boldsymbol{n}_{TT}$ – instantaneous NGS TT WFS readout, where $\mathcal{M}_{TT}$ is exact (infinite-dimensional) NGS TT WFS measurement operator, $\boldsymbol{n}_{TT}$ is the instantaneous NGS TT WFS noise readout.
- $\delta\boldsymbol{s}_{LO} = \mathcal{M}^{LO}\mathcal{P}_{LO}(\delta\boldsymbol{\phi}^{OI}_{NGS}) + \boldsymbol{n}_{LO}$ – instantaneous NGS LO WFS readout, where $\mathcal{M}_{LO}$ is exact (infinite-dimensional) NGS LO WFS measurement operator, $\boldsymbol{n}_{LO}$ is the instantaneous NGS LO WFS noise readout.
- $\boldsymbol{c}_{ASM} = \boldsymbol{c}^{TT}_{ASM} + \boldsymbol{c}^{LO}_{ASM} + \boldsymbol{c}^{HO}_{ASM}$ – instantaneous ASM control command vector consisting of tip/tilt (TT), low order (LO) and high order (HO) corrections.
- $\boldsymbol{c}_{DM} = \boldsymbol{c}^{LO}_{DM} + \boldsymbol{c}^{HO}_{DM}$ – instantaneous OI DM control command vector consisting of low and high order corrections.
- $\boldsymbol{c}_{LGS}$ – instantaneous LGS control command vector consisting of LGS WFS platform focus and rotation commands and the 6 LLT tip/tilt corrections.

9. The following projection operators are used for channel splitting:

- $\mathcal{P}^{HO}_{ST}$ – spatial high-pass projection operator acting on the $\delta\boldsymbol{\phi}^{HO}_{ST}$ wavefront.
- $\mathcal{P}^{LO}_{ST}$ – spatial low-pass projection operator acting on the $\delta\boldsymbol{\phi}^{HO}_{ST}$ wavefront.
- $\mathcal{P}^{HO}_{NGS}$ – spatial high-pass projection operator acting on the $\delta\boldsymbol{\phi}^{HO}_{NGS}$ wavefront.
- $\mathcal{P}^{LO}_{NGS}$ – spatial low-pass projection operator acting on the $\delta\boldsymbol{\phi}^{OI}_{NGS}$ wavefront.
- $\mathcal{P}^{TT}_{NGS}$ – spatial low-pass projection operator extracting tip/tilt from the $\delta\boldsymbol{\phi}^{OI}_{NGS}$ wavefront.

The vectors, matrices and operators listed above are the building blocks for the LTAO system control algorithms ans simulations. Below we elaborate on the internal structure of these objects.

6.5.2 Phase screens and propagation operators

As it was described in Sec. 6.3, the phase distribution vector $\vec{\phi}(\boldsymbol{x})$, is a concatenation of the turbulence distributions $\phi(\boldsymbol{x})$ on each phase screen, where $\boldsymbol{x}$ are the $(x, y)^t$-coordinates in the t-system (see Sec. 2) in the case of the phase screens being perpendicular to the telescope optical axis regardless of the pointing, which we will assume throughout this document. The phase distribution vector $\boldsymbol{\phi}(\boldsymbol{x})$ in the entrance pupil, where $\boldsymbol{x}$ are the pupil $(x, y)^t$-coordinates, is a concatenation of phase distributions corresponding to propagation from the several target or reference sources.

Because of the assumed linearity of the propagation operators, propagation operator matrices $\mathcal{T}$ or $\mathcal{R}$ are block $\#SRC \times \#PS$ matrix, where $\#SRC$ is the number of sources and $\#PS$ is the number of phase screens. Each block ij of the propagation matrix is a scalar propagation operator mapping phase distribution on the j^{th} phase screen to the entrance pupil propagated from i^{th} source. Thus, the operators involved in the GMT LTAO model are

- $\mathcal{T}_{ST}^{PS}$ is a $1 \times \#PS$-matrix;
- $\mathcal{R}_{LGS}^{PS}$ is a $6 \times \#PS$-matrix;
- $\mathcal{R}_{NGS}^{PS}$ is a $1 \times \#PS$-matrix;
- $\mathcal{T}_{ST}^{ASM}$ and $\mathcal{T}_{ST}^{DM}$ are 1×1-matrices and, to simplify equation for $\delta\boldsymbol{\phi}_{ST}^{OI}$, these two matrices can be concatenated into one 1×2-matrix $\mathcal{T}_{ST}^{OI}$;
- $\mathcal{R}_{NGS}^{ASM}$ and $\mathcal{R}_{NGS}^{DM}$ are 1×1-matrices and, to simplify equation for $\delta\boldsymbol{\phi}_{NGS}^{OI}$, these two matrices can be concatenated into one 1×2-matrix $\mathcal{R}_{NGS}^{OI}$.

The $\mathcal{T}$ and $\mathcal{R}$ propagation operators have especially simple form in case of the geometrical optics propagation (see Section 2):

$$\mathcal{H}(\boldsymbol{\phi}(\boldsymbol{x})) = \boldsymbol{\phi}(a\boldsymbol{x} + \boldsymbol{b}), \tag{6.5.1}$$

where $\mathcal{H}$ stands either for $\mathcal{T}$ or $\mathcal{R}$ and $(a, \boldsymbol{b})$ are computed from Eq. (2.5.4) for finite altitude point source (LGS) or Eq. (2.5.5) for infinite altitude point source (TS or NGS).

6.5.3 Projection operators

For the ideal channel split the following relations hold:

$$\mathcal{I} = \mathcal{P}_{ST}^{HO} + \mathcal{P}_{ST}^{LO}, \tag{6.5.2}$$

$$\mathcal{I} = \mathcal{P}_{NGS}^{HO} + \mathcal{P}_{NGS}^{LO} + \mathcal{P}_{NGS}^{TT}. \tag{6.5.3}$$

Thus, only three projection operators out of five need to be computed. Since all the splitting projection operators act on the wavefront phase from a single light source (ST or NGS) $\mathcal{P}$ are 1×1-matrices or just scalar operators.

Let an orthonormal basis $\boldsymbol{q}(\boldsymbol{x}) = \{q_i(\boldsymbol{x})\}_{i=1}^{\infty}$ be defined on the entrance pupil domain A with the basis functions $q_i(\boldsymbol{x})$. Then an orthogonal projector on a subset $\{q_i(\boldsymbol{x})\}_{i\in S}$ is

$$\mathcal{P}^S(\phi(\boldsymbol{x})) = \boldsymbol{q}_S^T[\boldsymbol{q}_S, \phi], \tag{6.5.4}$$

where $\boldsymbol{q}_S(\boldsymbol{x}) = \{q_i(\boldsymbol{x})\}_{i\in S}$, $[*,*]$ is the Hilbert space metric defined in Eq. (6.2.3). If the basis functions are sorted in ascending order with respect to the abundance of high order details, then the $\mathcal{P}^{TT}$-operators are made of $\{q_1, q_2\}$ (and, hopefully, $q_1(\boldsymbol{x})$ and $q_2(\boldsymbol{x})$ are indeed are very similar to tip and tilt, which is not guaranteed for a segmented aperture), the $\mathcal{P}^{TT}$-operators are made of $\{q_3, ..., q_{LO}\}$, etc.

6.6 ASM HO LGS controller algorithm

6.7 ASM LO NGS controller algorithm

6.8 ASM TT NGS controller algorithm

6.9 OI DM HO LGS controller algorithm

6.10 OI DM LO NGS controller algorithm

6.11 GMT LTAO system fusion

TBD

6.12 GMT LTAO system dynamic analysis

TBD

6.13 GMT LTAO system error and robustness analysis

TBD

7 Appendix: Matrix derivatives

Derivative of linear matrix functional

$$\boldsymbol{p}^T \mathcal{F} \boldsymbol{z}$$

with respect to matrix $\mathcal{F}$ is computed as follows:

1. Write the functional in element-wise form:

$$f = \boldsymbol{p}^T \mathcal{F} \boldsymbol{z} = \sum_i \sum_j p_i \mathcal{F}_{ij} z_j.$$

2. Differentiate with respect to $\mathcal{F}_{ij}$:

$$\frac{\partial f}{\partial \mathcal{F}_{ij}} = p_i z_j.$$

3. Thus

$$\frac{\partial}{\partial \mathcal{F}} (\boldsymbol{p}^T \mathcal{F} \boldsymbol{z}) = \boldsymbol{p} \boldsymbol{z}^T.$$

Derivative of quadratic matrix functional

$$\boldsymbol{z}^T \mathcal{F}^T \mathcal{A} \mathcal{F} \boldsymbol{z},$$

where $\mathcal{A}$ is symmetric real valued matrix, with respect to matrix $\mathcal{F}$ is computed as follows:

1. Write the functional in element-wise form:

$$f = \boldsymbol{z}^T \mathcal{F}^T \mathcal{A} \mathcal{F} \boldsymbol{z} = \sum_{i=1}^{m} \sum_{l=1}^{n} \sum_{j=1}^{m} \sum_{k=1}^{n} \mathcal{F}_{il} \mathcal{F}_{jk} \mathcal{A}_{ij} z_l z_k.$$

2. Most conveniently, by writing down the above equation for a case of small matrix size, say, 2x2, find by inspection that

$$\frac{\partial}{\partial \mathcal{F}} (\boldsymbol{z}^T \mathcal{F}^T \mathcal{A} \mathcal{F} \boldsymbol{z}) = 2 \mathcal{A} \mathcal{F} \boldsymbol{z} \boldsymbol{z}^T.$$

Analogously, the derivatives with respect to vector are:

$$\frac{\partial}{\partial \boldsymbol{z}} (\mathcal{F} \boldsymbol{z}) = \mathcal{F},$$

$$\frac{\partial}{\partial \boldsymbol{z}} \boldsymbol{z}^T \mathcal{F} \boldsymbol{z} = 2 \boldsymbol{z}^T \mathcal{F}.$$

8 Appendix: Basic discrete-time digital filter theory

Here the basic formulas for the digital linear filter theory are given.

Definition: a time-invariant, single-input-single-output (SISO), order N disctete-time linear digital filter is given by a linear, order-N difference equation with constant coefficients:

$$y(i) = \sum_{k=0}^{N} b_k u(i-k) - \sum_{k=1}^{N} a_k y(i-k),\ i = 0, ... \tag{8.0.1}$$

where i is *disctete time*, $u(i)$ is the *input sequence*, $y(i)$ is the *output sequence*. The filter in Eq. (8.0.1) is called *causal* because $y(i)$ does not depend on time instances $i+1$ and on. Appying z-transform to Eq. (8.0.1) one gets:

$$y(z)(1 + \sum_{k=1}^{N} a_k z^{-k}) = u(z) \sum_{k=0}^{N} b_k z^{-k}.$$

from where the *transfer function* is:

$$H(z) = \frac{y(z)}{u(z)} = b_0 + \frac{\sum_{k=1}^{N} \beta_k b_k z^{-k}}{1 + \sum_{k=1}^{N} a_k z^{-k}}, \tag{8.0.2}$$

$$\beta_k = b_k - b_0 a_k.$$

The canonical state-space model

$$\boldsymbol{x}(i+1) = \mathcal{A}\boldsymbol{x}(i) + \mathcal{B}\boldsymbol{u}(i), \tag{8.0.3}$$

$$\boldsymbol{y}(i) = \mathcal{C}\boldsymbol{x}(i) + \mathcal{D}\boldsymbol{u}(i)$$

describes the filter in terms of its internal state $\boldsymbol{x}(i)$ dynamics. The first equation is the *state dynamics equation*, the second is the *measurement equation*. The state space model parameters for the filter are easily derivable from Eq. (8.0.2):

$$\boldsymbol{u}(i) = [u(i)], \tag{8.0.4}$$

$$\boldsymbol{y}(i) = [y(i)],$$

$$\mathcal{A} = \begin{bmatrix} -a_1 & -a_2 & \cdots & -a_{N-1} & -a_N \\ 1 & 0 & \cdots & 0 & 0 \\ 0 & 1 & \cdots & 0 & 0 \\ \vdots & \vdots & \ddots & \vdots & \vdots \\ 0 & 0 & \cdots & 1 & 0 \end{bmatrix}$$

$$\mathcal{B} = [1 \cdots 0]^T,$$

$$\mathcal{C} = [\beta_1 \cdots \beta_N],$$

$$\mathcal{D} = [b_0].$$

9 Appendix: Theory of Generalized Fresnel Transform

Generalized Fresnel Transform (GFT) is a Fresnel diffraction integral generalized to propagation through a paraxial optic system defined through the *wave-* or *ABCD*-matrix [9, 10]

$$W = \begin{bmatrix} A & B \\ C & D \end{bmatrix}, \ |W| = AD - BC = 1. \tag{9.0.5}$$

The GFT is defined as

$$U(\boldsymbol{y}) = \mathbb{F}[A,B,D]\{U(\boldsymbol{x})\}(\boldsymbol{y}) = \tag{9.0.6}$$
$$\frac{e^{ikz}}{i\lambda B}\int_{-\infty}^{\infty} U(\boldsymbol{x}) \exp\left[i\frac{k}{2B}(A|\boldsymbol{x}|^2 - 2\boldsymbol{x}^T\boldsymbol{y} + D|\boldsymbol{y}|^2)\right] d\boldsymbol{x}, \ k = \frac{2\pi}{\lambda},$$

where $\boldsymbol{x}, \boldsymbol{y}$ are the xy-coordinates in the source and observation planes, respectively, z is the distance between the planes, U is a complex amplitude of the scalar field at the planes. Obviously, when considering free-space propagation, i.e. when

$$W = \begin{bmatrix} 1 & z \\ 0 & 1 \end{bmatrix}, \tag{9.0.7}$$

Eq. (9.0.6) turns into classical Fresnel diffraction integral. Ref. [10] develops theory of the GFT in the form of several theorems. We give here a subset of the most useful GFT theorems translated from 1D to 2D case.

Cast-to-convolution theorem.
At first glance Eq. (9.0.6) does not look like a convolution but it is possible to reduce it to convolution after change of variables:

$$U(\boldsymbol{y}) = \frac{e^{ikz}}{i\lambda B}\exp\left(i\frac{kC}{2A}|\boldsymbol{y}|^2\right)\int_{-\infty}^{\infty} U(\boldsymbol{x})\exp\left(i\frac{kA}{2B}|\frac{\boldsymbol{y}}{A} - \boldsymbol{x}|^2\right) d\boldsymbol{x}. \tag{9.0.8}$$

This theorem allows to use Fast Fourier Transform for computing GFTs. The convolution kernel in Eq. (9.0.8), the *GFT chirp*, has analytical Fourier Transform:

$$\mathcal{F}\{\exp\left(i\frac{kA}{2B}|\boldsymbol{x}|^2\right)\}(\boldsymbol{f}) = \frac{i}{\alpha}\exp\left[-i\frac{\pi}{\alpha}|\boldsymbol{f}|^2\right], \ \alpha = \frac{A}{\lambda B}. \tag{9.0.9}$$

Eq. (9.0.8) has simple interpretation: propagation through optical system described by an ABCD-matrix consists of 3 steps

1. Free space propagation by distance B/A (convolution term in Eq. (9.0.8)).
2. Scaling the propagation result by magnification A. If, for instance, the first step is done through FFT on a discrete grid with spacing dx in the source plane, then in the observation plane the grid spacing is equal to Adx.
3. Multiplication by a phase mask corresponding to negative thin lens with focal distance $f = -A/C$.

Shift theorem.

$$\mathbb{F}[A,B,D]\{U(\boldsymbol{x} - \boldsymbol{x}_0)\}(\boldsymbol{y}) = \exp\left[i\frac{k}{2}C\boldsymbol{x}_0^T(2\boldsymbol{y} - A\boldsymbol{x}_0)\right]\mathbb{F}[A,B,D]\{U(\boldsymbol{x})\}(\boldsymbol{y} - A\boldsymbol{x}_0). \tag{9.0.10}$$

Tilt theorem.

$$\mathbb{F}[A,B,D]\{U(\boldsymbol{x})\exp[ik\boldsymbol{x}_0^T\boldsymbol{x}]\}(\boldsymbol{y}) = \exp\left[ikD\boldsymbol{x}_0^T(\boldsymbol{y}-\frac{B}{2}\boldsymbol{x}_0)\right]\mathbb{F}[A,B,D]\{U(\boldsymbol{x})\}(\boldsymbol{y}-B\boldsymbol{x}_0). \quad (9.0.11)$$

Focus theorem.

$$\mathbb{F}[A,B,D]\{U(\boldsymbol{x})\exp\left[i\frac{k}{2f}|\boldsymbol{x}|^2\right]\}(\boldsymbol{y}) = \mathbb{F}[A+\frac{B}{f},B,D]\{U(\boldsymbol{x})\}(\boldsymbol{y}). \quad (9.0.12)$$

Note that, to keep the wave matrix unimodular after $A' = A + \frac{B}{f}$ transformation, the C-coeffficient has to be transformed into

$$C' = C + \frac{D}{f}. \quad (9.0.13)$$

Shift, tilt and focus theorems allow to factor possibly highly oscillating terms out of the integral. To see this for focus theorem, Eq. (9.0.12) needs to be substituted into Eq. (9.0.8).

10 Bibliography

References

[1] O. Lardiere, R. Conan, R. Clare, C. Bradley, N. Hubin, "Performance comparison of centroiding algorithms for laser guide star wavefront sensing with extremely large telescopes," *Appl. Opt.*, **49**, G78-G94 (2010).

[2] D. M. Wiberg, C. E. Max, and D. T. Gavel, "A spatial non-dynamic LQG controller: Part 1, Application to adaptive optics," in *Proceedings of the 2004 IEEE Conference on Decision and Control* (IEEE, 2004), pp. 3326 - 3332.

[3] D. M. Wiberg, C. E. Max, and D. T. Gavel, "A spatial non-dynamic LQG controller: Part 2, Theory," in *Proceedings of the 2004 IEEE Conference on Decision and Control* (IEEE, 2004), pp. 3333 - 3338.

[4] D. M. Wiberg, C. E. Max, and D. T. Gavel, "Geometric view of adaptive optics control," JOSA A, Vol. 22, pp. 870 - 880 (2004).

[5] L. A. Poyneer, B. Macintosh, "Spatially filtered wave-front sensor for high-order adaptive optics," JOSA A, Vol. 21, Issue 5, pp. 810-819 (2004).

[6] *Giant Magellan Telescope. Laser Tomography Adaptive Optics. Conceptual Design Review.* Research School of Astronomy and Astrophysics, The College of Physical and Mathematical Science, The Australian National University.
GMTO Document Number: GMT-01-00140. (2011)

[7] Rodolphe Conan, *GMT Mathematics Handbook.* Personal communication.
rconan@mso.anu.edu.au

[8] R. Upton, B. Ellerbroek, "GramSchmidt orthogonalization of the Zernike polynomials on apertures of arbitrary shape," Opt. Lett., Vol. 29, pp. 2840 – 2842, (2004).

[9] J. D. Schmidt, *Numerical Simulation of Optical Wave Propagation With examples in MATLAB*, SPIE (2010).

[10] C. Palma, V. Bagini, "Extension of the Fresnel transform to ABCD systems," JOSA A, Vol. 14, pp. 1774 – 1779 (1997).

Index